PEOPLES DEMOCRATIC REPUBLIC OF ALGERIA
MINISTRY OF HIGHER EDUCATION AND SCIENTIFIC RESEARCH

Mohamed Boudiaf University of M'Sila
Faculty of Mathematics and Computer Science
Department of Mathematics

Master memory

Field: Mathematics and Computer Science
Department : Mathematics
Option : Partial Differential Equations and Applications

Theme

PDE-Based Geodesic Active Contours for Image Segmentation

Presented by:
RADJAI Rahma

Publicly defended on : September 24, 2026

In front of the jury composed of:

BENHAMIDOUCHE Noureddine	Prof ,	M'sila University	**Chairperson**
CHOUDER Rafaa	MCA ,	M'sila University	**Supervisor**
BASTI Bilal	MCA ,	M'sila University	**Examiner**

University year 2025/2026

Contents

Introduction 1

1 *Preliminaries and Basic Definitions* **3**

1.1 Introduction to Image Processing . . . 3

1.1.1 The Image Society . . . 3

1.1.2 Mathematical Definition of an Image . . . 4

1.1.3 What is Image Processing ? . . . 5

1.2 Image Derivatives, Gradients and Edge Detection . . . 7

1.3 Elements of Differential Geometry: Curvature . . . 12

1.4 Partial Differential Equations . . . 17

1.5 Level Set Method . . . 20

2 *Geodesic Active Contours Model* **23**

2.1 The Kass-Witkin-Terzopoulos Snake Model . . . 23

2.2 The Geodesic Active Contours Model . . . 26

2.2.1 Geometric Motivation . . . 26

2.2.2 Interpretation of the Geodesic Flow . . . 32

2.3 The Level-Set Method . . . 34

3 Numerical Implementation and Experiments **45**

3.1 Finite Differences Discretization . . . 45

3.2 Numerical Scheme for the Geodesic Active Contour . . . 46

3.3 Experimental Results . . . 49

Conclusion **54**

Bibliography **56**

Acknowledgments

First of all, I would like to thank **"Allah"** the all-powerful, for having given us strength and patience since born in this life.

I am grateful to my supervisor, Mr. **Rafaa Chouder** for their accurate guidance, support, and suggestions that made for this work. Their valuable advice carried me through every stage of writing my memory. It is truly impossible to adequately express my appreciation to them in mere words.

I extend my respect and gratitude to the members of the Jury, Dr. **Noureddine Benhamidouche** and Dr. **Bilal Basti**, for graciously agreeing to examine and evaluate my work. Their insightful remarks and suggestions will undoubtedly contribute to enhancing the quality of this memory.

My family, especially my parents, played an indispensable role in the completion of this work. Their unwavering support and encouragement have been invaluable.

Last but not least, I would like to express my gratitude to all my teachers and everyone who has directly or indirectly contributed to the realization of this work.

Abstract

This memory studies the *Geodesic Active Contour* (GAC) model, a geometric, PDE-based approach to image segmentation. After recalling the necessary background in image processing, differential geometry, and partial differential equations, we show how the classical Kass–Witkin–Terzopoulos snake model, limited by its dependence on curve parametrization, is reformulated by Caselles, Kimmel, and Sapiro as a weighted-length minimization problem. The resulting evolution combines a curvature-driven regularizing force with an edge-driven attraction force and a balloon term. Rewritten within the level set framework as a Hamilton–Jacobi-type equation, the model is shown to admit a unique, stable viscosity solution whose zero level set converges to the true object boundary.

A numerical scheme is then designed, using central finite differences for the curvature term and monotone upwind (Godunov-type) schemes for the hyperbolic terms. Experiments on synthetic images, real images, and challenging cases confirm the effectiveness of the model on well-contrasted boundaries, while revealing its limitations when image gradients are weak or ambiguous.

Keywords: Image segmentation, Geodesic active contours, Partial differential equations, Level set method, Curvature flow, Viscosity solutions, Finite differences, Upwind schemes.

ملخص

تتناول هذه المذكرة نموذج **العتبات النشطة الجيوديزية** (GAC) ، وهو نهج هندسي لتجزيء الصور يعتمد على المعادلات التفاضلية الجزئية. بعد استعراض الأدوات الرياضية اللازمة (معالجة الصور، الهندسة التفاضلية، المعادلات التفاضلية الجزئية)، نبيّن كيف أن نموذج Kass-Witkin-Terzopoulos الكلاسيكي (Snake) ، المحدود بسبب اعتماده على بارامترة المنحنى، أُعيدت صياغته هندسيًا من طرف Caselles ; Kimmel ; Sapiro كمسألة تصغير لطول موزون. يجمع التدفق التطوري الناتج بين قوة تنعيم مرتبطة بالانحناء وقوة جذب نحو الحواف وحد إضافي يُعرف بقوة البالونْ. وبإعادة صياغته ضمن إطار مجموعات المستوى كمعادلة من نوع هاميلتو نجاكوبي، نثبت وجود ووحدانية واستقرار حله بمفهوم الحلول اللزجة، مع تقارب المنحنى نحو الحد الحقيقي للجسم.

كما صُمم مخطط عددي يجمع بين الفروق المتنهية المركزية لحد الانحناء ومخططات الصعود (Upwind) من نوع Godunov للحدود الزائدية. وأكدت التجارب على صور اصطناعية وحقيقية وحالات صعبة فعالية النموذج عند وضوح الحدود، مع إبراز حدوده عند ضعف أو تنافس تدرجات الصورة.

الكلمات المفتاحية: تجزيء الصور، العتبات النشطة الجيوديزية، المعادلات التفاضلية الجزئية، طريقة مجموعات المستوى، تدفق الانحناء، الحلول اللزجة، الفروق المتنهية، مخططات الصعود (Upwind) .

Introduction

Image segmentation, the partitioning of an image into meaningful regions, is a fundamental problem in image processing and computer vision, since the quality of the extracted boundaries conditions all subsequent analysis [1]. Among the many approaches proposed over the years, *active contour* models have played a central role: an initial curve is deformed until it converges toward the boundaries of the objects of interest. This idea was first formalized by Kass, Witkin, and Terzopoulos through the *snake* model [7], which minimizes an energy combining an internal regularity term and an external term derived from the image gradient. However, this classical model depends explicitly on the parametrization of the curve, handles topological changes poorly, and is numerically unstable when the deformation becomes large.

To overcome these limitations, Caselles, Kimmel, and Sapiro introduced the *Geodesic Active Contour* (GAC) model [4], which reinterprets object boundaries as geodesics of minimal length with respect to a Riemannian metric induced by the image; a closely related geometric formulation was also proposed by Caselles, Catté, Coll, and Dibos [3], and by Kichenassamy et al. [8, 9] under the name of conformal/geometric active contours. Combined with the *level set method* of Osher and Sethian [12], which represents the evolving curve implicitly as the zero level set of a higher-dimensional function, this reformulation removes the dependence on parametrization and naturally accommodates topological changes, as further developed by Malladi, Sethian, and Vemuri [11] and detailed in the monographs of Sethian [14] and Sapiro [13].

This memory is devoted to the theoretical study and numerical implementation of the GAC model, viewed as a partial differential equation of Hamilton–Jacobi type. It is organized into three chapters.

Chapter 1 introduces the mathematical background needed throughout the memory: basic notions of image processing and edge detection, elements of differential geometry with emphasis on curvature, and the essential theory of partial differential equations [6], together with the level set method [12, 14].

Chapter 2 constitutes the theoretical core of the work. It presents the Kass–Witkin–Terzopoulos snake model [7] and its limitations, derives the geodesic active contour model [4] as a geometric reformulation of the snake energy following the equivalence result of Aubert and Blanc-Féraud [2], and analyzes the resulting evolution equation as a competition between curvature-driven smooth-

ing and edge-driven attraction, complemented by a balloon force. The level set formulation of the model is then studied in the framework of viscosity solutions, following the analysis of Caselles, Catté, Coll, and Dibos [3], establishing existence, uniqueness, stability, and convergence of the evolving contour toward the true object boundary.

Chapter 3 addresses the numerical implementation of the model, using central finite differences for the curvature (parabolic) term and monotone upwind (Godunov-type) schemes for the hyperbolic propagation and advection terms, in the spirit of the numerical front-propagation techniques of Osher and Sethian [12] and Dervieux and Thomasset [5]. The resulting scheme is validated through experiments on synthetic images, real images, and challenging cases.

كلية الرياضيات والإعلام
Faculté des Mathématiques et de l'Informatique

Chapter 1

Preliminaries and Basic Definitions

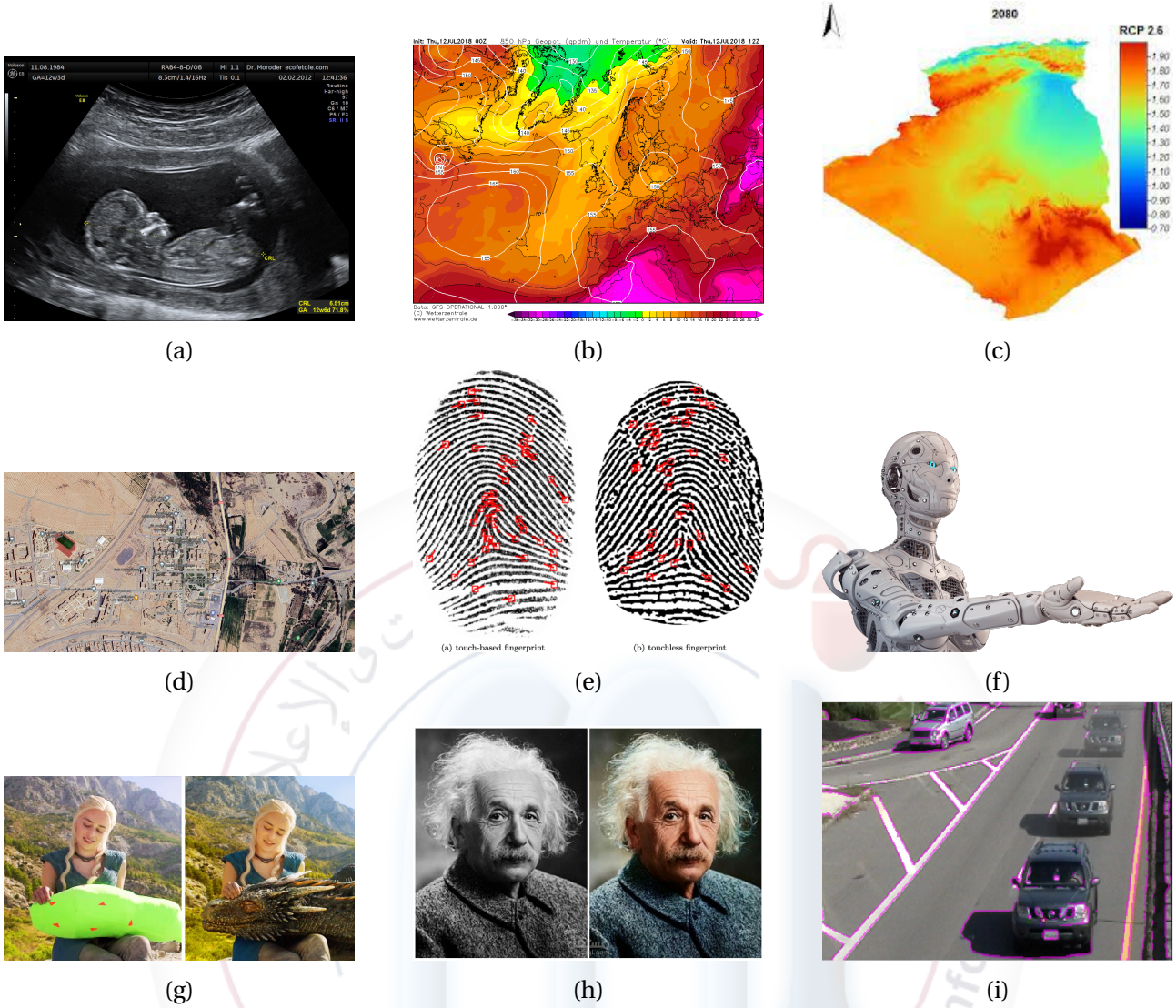
The goal of this chapter is to introduce the fundamental concepts of image processing and to present the mathematical tools that will be used throughout the subsequent chapters. It provides the necessary background for the study of Geodesic Active Contours by first presenting basic notions of image representation, gradients, and edge detection. It then introduces essential elements of differential geometry, with particular emphasis on curvature and geometric flows that govern contour evolution. Finally, it discusses partial differential equations and the level set method as the main analytical and computational framework for modeling moving interfaces in image segmentation.

1.1 Introduction to Image Processing

1.1.1 The Image Society

In our rapidly evolving world, society can aptly be described as an image society. This designation is not only due to the power and significance of images as a means of communication, but also because of their ease of use, compact nature, and widespread popularity. Images are used by people everywhere to describe, express, and represent the physical world. They capture moments and events, freezing them in time and allowing us to analyse and enhance their quality, highlight specific characteristics, and efficiently combine different pieces of information. From advertising and photography to video games, images permeate our daily lives.

Moreover, there are numerous applications where image processing is integral; almost every area of science and technology can make use of image processing methods. Examples include medical imaging, satellite and aerial imaging, weather forecasting, fingerprint analysis, robotics, quality control, multimedia data management, video processing, and the restoration of old movies, among others (See Figure 1.1). Whether we realize it or not, we are consumers of image processing technology on a daily basis.



(a) (b) (c)

(d) (e) (f)

(g) (h) (i)

Figure 1.1: Some applications where image processing is concerned.

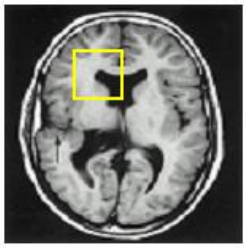
1.1.2 Mathematical Definition of an Image

In image processing, a continuous Gray-scale image is considered that is a two-dimensional function

$$\begin{aligned} u \quad &: \quad \mathbb{R}^2 \to \mathbb{R} \\ &\quad (x,y) \to u(x,y) \end{aligned}$$

The variable (x,y), for digital images, actually belongs to $\mathbb{N}^2$, it is a pixel of the image. $u(x,y)$ represents the luminous intensity, or the Gray level of the image at the pixel (x,y).

Digital images are most commonly presented as a matrix of scalars for gray-scale images or vectors for colour images. Digital Gray scale images on the other hand are sampled and quantized. Sampling is the discretization of the image domain. Here an image consists of Gray values of a rectangular point grid $\{u_{i,j} \setminus \ i = 0,...,N-1 \text{ and } j = 0,...,M-1\}$. A grid point (i,j) is called pixel. Here N and M are the width and height of the image in pixels, respectively. $u_{i,j}$ denotes the Gray



125	131	147	171	173	154	145	128	123
121	124	142	163	169	161	147	135	128
135	131	139	148	155	163	155	144	138
150	150	141	146	150	155	158	157	158
193	189	171	161	162	167	176	182	188
197	207	204	199	198	199	203	205	206
183	202	215	222	219	217	217	214	208
181	198	210	216	218	217	217	37	22
180	197	209	213	216	212	212	91	25
191	201	211	215	214	208	208	21	23
206	208	210	215	215	211	212	16	14

Figure 1.2: Gray level digital image

value of pixel (i, j). (See Figure 1.2).

For a colour image, it is not enough to know its Gray level for each pixel: it is necessary to know the intensity of each of the three channels of the fundamental colours, the red R, the green G, and the blue B. A colour image can then be defined as a vector function, (See Figure 1.3),

$$\begin{aligned} u \quad &: \quad \mathbb{R}^2 \to \mathbb{R}^3 \\ &\quad (x, y) \to u(x, y) = (R(x, y); G(x, y); B(x, y)). \end{aligned}$$

1.1.3 What is Image Processing ?

Image processing is a branch of computer science and applied mathematics concerned with the analysis, enhancement, and manipulation of digital images. Its primary objective is to transform images into a form that is either more suitable for human interpretation or more appropriate for subsequent automated analysis.

Closely related to image processing is the field of computer vision, whose goal is to extract meaningful information from visual data and to emulate, as much as possible, the capabilities of the human visual system. Computer vision involves higher-level tasks such as image segmentation, object recognition, three-dimensional reconstruction, motion analysis, and scene understanding. To accomplish these tasks, computer vision systems often rely on image processing techniques combined with machine learning, variational methods, optimization techniques, and geometric approaches.

In contrast, image processing mainly focuses on improving the quality of images or extracting relevant low-level information from them. Typical image processing tasks include:

- **Feature extraction:** Detecting important image structures such as edges, corners, ridges, and texture patterns, which play a crucial role in visual perception and subsequent analysis.



$RED ==$

124	120	116	116	114	120	125	100	105	128	119
122	117	115	114	112	112	116	89	95	120	113
118	115	113	113	112	111	114	87	93	119	112
120	117	115	116	114	110	113	85	92	117	109
155	155	149	148	152	153	147	141	139	143	147
178	178	173	172	175	180	176	172	170	173	174

$GREEN ==$

145	141	139	139	137	139	142	114	118	141	136
141	138	135	137	135	132	135	106	109	134	132
137	134	133	133	132	136	137	107	112	138	135
139	136	135	136	134	138	138	108	112	137	134
147	147	141	140	144	144	138	132	132	136	140
166	166	161	160	163	167	163	159	160	163	166

$BLUE ==$

150	146	145	145	143	146	150	123	127	150	144
147	143	142	143	141	139	142	114	118	143	139
143	140	140	140	139	141	143	114	119	145	141
145	142	142	143	141	142	143	114	119	144	139
136	136	130	129	133	135	129	123	122	126	130
154	154	149	148	151	158	154	150	150	153	155

Figure 1.3: Color image

- **Image segmentation:** Partitioning an image into homogeneous regions with similar characteristics, while accurately locating the boundaries between different objects or regions.
- **Image deblurring:** Recovering a sharp image from a blurred observation by compensating for image degradation caused by motion, defocus, or other acquisition imperfections.
- **Image denoising:** Removing unwanted noise while preserving significant image details such as edges and fine structures.
- **Image enhancement:** Improving visual quality through contrast adjustment, histogram equalization, sharpening, and other enhancement techniques.

Image processing constitutes the foundation of many modern applications, including medical imaging, remote sensing, surveillance systems, industrial inspection, autonomous vehicles, and multimedia technologies.
Among all image processing tasks, image segmentation occupies a central position because it provides the first step toward object extraction and scene understanding. The Geodesic Active Contour model studied in this dissertation belongs to this class of segmentation techniques and relies heavily on partial differential equations and differential geometry.

1.2 Image Derivatives, Gradients and Edge Detection

The detection of object boundaries is a fundamental task in image processing and computer vision. Most image segmentation methods rely on the observation that significant intensity variations often correspond to object edges. Consequently, differential operators play a central role in extracting boundary information from images.
The gradient is one of the most important mathematical tools for measuring local intensity variations. It provides both the magnitude and direction of the strongest intensity change and therefore serves as the basis for many edge detection techniques. In Geodesic Active Contour models, image gradients are used to construct edge indicator functions that guide the contour evolution toward object boundaries.

Image Derivatives

Let $I : \Omega \subset \mathbb{R}^2 \to \mathbb{R}$ be a grayscale image defined on the domain Ω.
The first-order partial derivatives of the image are

$$I_x = \frac{\partial I}{\partial x}, \qquad I_y = \frac{\partial I}{\partial y}.$$

These derivatives measure the rate of intensity variation along the horizontal and vertical directions, respectively.

For a discrete image, derivatives are approximated numerically. The forward difference approximations are given by

$$I_x(i,j) \approx I(i+1,j) - I(i,j),$$

and

$$I_y(i,j) \approx I(i,j+1) - I(i,j).$$

More accurate approximations are obtained using centered differences:

$$I_x(i,j) \approx \frac{I(i+1,j) - I(i-1,j)}{2},$$

$$I_y(i,j) \approx \frac{I(i,j+1) - I(i,j-1)}{2}.$$

These approximations constitute the basis of many numerical edge detection operators.

Derivative Filters

Numerical differentiation can also be interpreted as a convolution operation. For example, the centered difference approximation in the horizontal direction corresponds to the convolution kernel

$$D_x = \frac{1}{2}\begin{bmatrix} -1 & 0 & 1 \end{bmatrix},$$

while the vertical derivative is obtained using

$$D_y = \frac{1}{2}\begin{bmatrix} -1 \\ 0 \\ 1 \end{bmatrix}.$$

This convolutional interpretation provides the basis for most practical edge detection operators.

Gradient Magnitude and Orientation

The image gradient is defined as

$$(I_x, I_y).$$

The gradient vector points in the direction of the maximum increase of image intensity.

The gradient magnitude is defined by

$$\sqrt{I_x^2 + I_y^2}.$$

The magnitude measures the strength of local intensity variations. Regions with nearly constant intensity correspond to small gradient values, whereas edges correspond to large gradient magnitudes.

The orientation of the gradient is given by

$$\tan^{-1}\left(\frac{I_y}{I_x}\right).$$

This angle indicates the direction of the steepest intensity increase.

Since image edges are characterized by abrupt intensity transitions, they are generally associated with local maxima of the gradient magnitude.

Gradient-Based Interpretation of Edges

Consider a one-dimensional intensity profile $I(x)$. In a homogeneous region, $I(x)$ = constant, and therefore

$$\frac{dI}{dx} = 0.$$

At an edge location, the intensity changes rapidly, leading to

$$\left|\frac{dI}{dx}\right| \gg 0.$$

This observation naturally extends to two-dimensional images through the gradient norm $|\nabla I|$.

Consequently, edges may be identified as locations where the gradient magnitude reaches local maxima.

In practice, image edges correspond to discontinuities or sharp transitions in the image intensity function. These discontinuities may arise from changes in object reflectance, illumination, texture, or depth. Detecting such transitions is therefore a key step in many segmentation and object extraction algorithms.

Second-Order Derivatives and the Laplacian

Second-order derivatives provide complementary information about image structures.

The Laplacian operator is defined by

$$\frac{\partial^2 I}{\partial x^2} + \frac{\partial^2 I}{\partial y^2}.$$

The Laplacian measures the local curvature of the image intensity surface.

Zero-crossings of the Laplacian of a smoothed image often indicate the presence of edges. This observation constitutes the basis of the Laplacian-of-Gaussian edge detector.

Laplacian of Gaussian (LoG)

To improve robustness against noise, the image is first smoothed by a Gaussian kernel and then differentiated using the Laplacian operator. The resulting operator is known as the Laplacian of Gaussian (LoG):

$$\Delta(G_\sigma * I).$$

Edges are detected as zero-crossings of the filtered image.

Classical Edge Detection Operators

Several numerical operators have been proposed to estimate image gradients.

Roberts Operator

The Roberts operator uses the masks

$$G_x = \begin{bmatrix} 1 & 0 \\ 0 & -1 \end{bmatrix}, \qquad G_y = \begin{bmatrix} 0 & 1 \\ -1 & 0 \end{bmatrix}.$$

Although computationally efficient, the Roberts operator is sensitive to noise.

Prewitt Operator

The Prewitt masks are

$$G_x = \begin{bmatrix} -1 & 0 & 1 \\ -1 & 0 & 1 \\ -1 & 0 & 1 \end{bmatrix},$$

$$G_y = \begin{bmatrix} -1 & -1 & -1 \\ 0 & 0 & 0 \\ 1 & 1 & 1 \end{bmatrix}.$$

These masks incorporate local averaging and improve robustness against noise.

Sobel Operator

The Sobel operator is one of the most widely used gradient estimators. The corresponding convolution kernels are

$$G_x = \begin{bmatrix} -1 & 0 & 1 \\ -2 & 0 & 2 \\ -1 & 0 & 1 \end{bmatrix},$$

$$G_y = \begin{bmatrix} -1 & -2 & -1 \\ 0 & 0 & 0 \\ 1 & 2 & 1 \end{bmatrix}.$$

The additional weighting in the central row and column provides improved noise suppression.

Canny Edge Detector

The Canny detector is widely regarded as one of the most effective edge detection methods. Its procedure consists of four stages:

1. Gaussian smoothing;
2. Gradient computation;
3. Non-maximum suppression;
4. Hysteresis thresholding.

This method achieves good localization, low detection error, and a single response per edge.

Gaussian Smoothing

Since differentiation amplifies noise, gradient computation is usually preceded by image smoothing. The Gaussian kernel is defined as

$$\frac{1}{2\pi\sigma^2}\exp\left(-\frac{x^2+y^2}{2\sigma^2}\right).$$

The smoothed image is obtained by convolution:

$$G_\sigma * I.$$

The parameter σ controls the amount of smoothing.
Small values of σ preserve fine image details, whereas larger values provide stronger noise reduction.

Why Gradients are Important for Active Contours

Active contour models rely on image gradients to determine the location of object boundaries. Strong gradients indicate likely edge locations and generate forces that attract the evolving contour toward the desired boundary.
Consequently, the quality of gradient estimation directly affects the accuracy of contour evolution. For this reason, gradient computation is usually performed on a smoothed image rather than on the raw image data.

Edge Indicator Functions

Geodesic Active Contour models use edge indicator functions derived from image gradients. A commonly used function is

$$\frac{1}{1+s^2},$$

where $s = |\nabla I_\sigma|$. Thus,

$$\frac{1}{1+|\nabla I_\sigma|^2}.$$

The original formulation used in Geodesic Active Contours is often written as

$$\frac{1}{1+\lambda s^2}, \qquad \lambda > 0,$$

where λ controls the sensitivity of the detector to image gradients.
These functions satisfy $0 < g \leq 1$. In homogeneous regions, $|\nabla I_\sigma| \approx 0$, which implies $g \approx 1$. Near strong edges, $|\nabla I_\sigma| \gg 1$, and therefore $g \approx 0$.
Another frequently used edge indicator is $g(s) = e^{-s^2}$. Both functions decrease rapidly near image boundaries and play a fundamental role in active contour models.

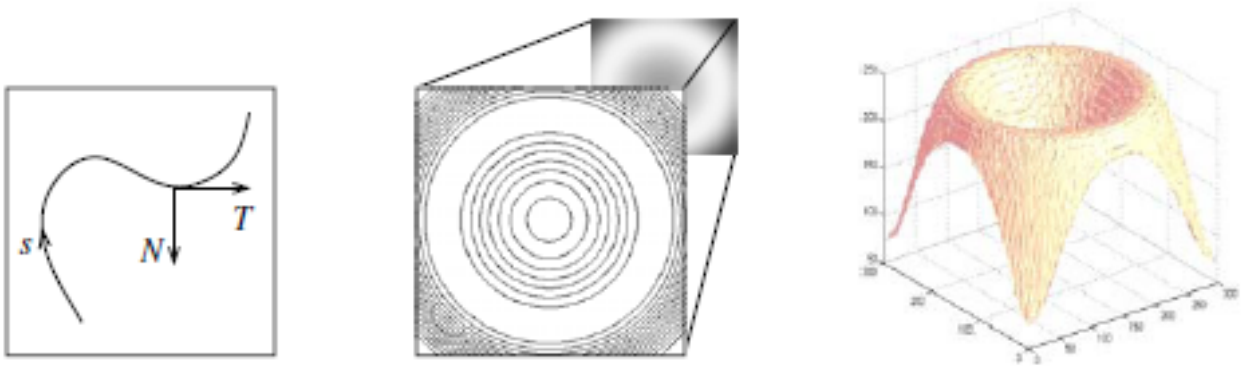


Figure 1.4: Different "objects" encountered in image analysis: parametrized curves, curves as Level Sets of an image, image as a surface.

Role of Image Gradients in Geodesic Active Contours

The gradient field establishes the connection between image information and contour evolution. In Geodesic Active Contour models, edge indicator functions modify the geometry of the image domain such that object boundaries correspond to regions of minimal propagation speed. As a result, the evolving contour naturally converges toward image edges while preserving geometric regularity.

The concepts introduced in this section constitute the mathematical foundation for the derivation of the Geodesic Active Contour model presented in Chapter 2.

1.3 Elements of Differential Geometry: Curvature

In this section we recall some basic definitions and properties of differential geometry and focus on the notion of curvature. Curvature has different meanings depending on the "object" that we are considering. We shall define the notion of curvatures for:

- Parametrized curves (for snakes, for instance),
- Images that can be represented by their isovalues,
- Images seen as surfaces where the height is the gray-scale intensity (see Figure 1.4).

Parametrized Curves

Let $x(p) = \big(x_1(p), x_2(p)\big)$ be a regular planar oriented curve in $\mathbb{R}^2$, $0 < p < 1$. We denote

$$
\begin{aligned}
&T(p) = x'(p) = \big(x_1'(p), x_2'(p)\big), \text{ the tangent vector at } x(p),\\
&N(p) = \big(-x_2'(p), x_1'(p)\big), \text{ the normal vector at } x(p),\\
&s(p) = \int_0^p \sqrt{\big(x_1'(r)\big)^2 + \big(x_2'(r)\big)^2}\, dr, \text{ the curvilinear abscissa (or arc length).}
\end{aligned}
$$

If $x(p)$ is regular, we can parametrize it by s, and then $T(s) = \frac{dx}{ds}(s)$ is such that $|T(s)| = 1$. The curvature vector is $\frac{dT}{ds}$, and since $T = \frac{dx}{ds}$, we have

$$\frac{dT}{ds} = \frac{d^2x}{ds^2}.$$

One can show that the curvature vector is collinear to $\dfrac{N(s)}{|N(s)|}$, i.e.,

$$\frac{dT}{ds}(s) = \kappa(s)\,\frac{N(s)}{|N(s)|},$$

where $\kappa(s)$ is the curvature and $\frac{1}{|\kappa(s)|}$ is the radius of curvature.

For any parametrization we have

$$\kappa(p) = \frac{x_1'(p)\,x_2''(p) - x_2'(p)\,x_1''(p)}{\left((x_1'(p))^2 + (x_2'(p))^2\right)^{3/2}}. \tag{1.1}$$

Moreover,

$$\frac{1}{|x'(p)|}\,\frac{\partial}{\partial p}\left(\frac{x'(p)}{|x'(p)|}\right) = \kappa(p)\left(\frac{N(p)}{|N(p)|}\right). \tag{1.2}$$

Curves as Level Sets of a Function u

Let us now consider the case where $x(s)$, parametrized by its curvilinear abscissa, is the k-level set of a function

$$u : \mathbb{R}^2 \to \mathbb{R},$$

that is,

$$x(s) = \{(x_1(s), x_2(s))\ ;\ u(x_1(s), x_2(s)) = k\}.$$

By differentiating the equality $u(x_1(s), x_2(s)) = k$ with respect to s, we obtain

$$x_1'(s)\,u_{x_1} + x_2'(s)\,u_{x_2} = 0. \tag{1.3}$$

where u_{x_1} stands for $\frac{\partial u}{\partial x_1}\big(x_1(s), x_2(s)\big)$. Therefore, the vectors $\big(x_1'(s), x_2'(s)\big)$ and $(-u_{x_2}, u_{x_1})$ are collinear. For some λ we have

$$\begin{cases} x_1'(s) = -\lambda u_{x_2}, \\ x_2'(s) = \lambda u_{x_1}, \end{cases} \tag{1.4}$$

so the vectors (u_{x_1}, u_{x_2}) and $(-u_{x_2}, u_{x_1})$ are respectively normal and tangent to the curve $x(s)$.

If we differentiate again (1.3) with respect to s, we obtain

$$(x_1'(s))^2 u_{x_1x_1} + (x_2'(s))^2 u_{x_2x_2} + 2x_1'(s)x_2'(s)u_{x_1x_2} + x_1''(s)u_{x_1} + x_2''(s)u_{x_2} = 0.$$

Using (1.4), this becomes

$$\lambda^2\left((u_{x_1})^2 u_{x_2x_2} + (u_{x_2})^2 u_{x_1x_1} - 2u_{x_1}u_{x_2}u_{x_1x_2}\right) + \frac{1}{\lambda}\left(x_1''(s)x_2'(s) - x_2''(s)x_1'(s)\right) = 0.$$

Since $|x'(s)| = 1$, we obtain from (1.4) $\lambda^2 = \frac{1}{|\nabla u|^2}$.

Therefore, using (1.1), we deduce the expression of the curvature (of course we assume $|\nabla u(x)| \neq 0$):

$$\kappa = \frac{(u_{x_1})^2 u_{x_2x_2} + (u_{x_2})^2 u_{x_1x_1} - 2u_{x_1}u_{x_2}u_{x_1x_2}}{\left((u_{x_1})^2 + (u_{x_2})^2\right)^{3/2}}. \tag{1.5}$$

The curvature can be expressed as

$$\kappa = \operatorname{div}\left(\frac{\nabla u}{|\nabla u|}\right). \tag{1.6}$$

This formula shows that the curvature of a level set can be computed directly from the image function without an explicit parametrization of the curve. This property is fundamental in level set methods and geometric active contours.

This expression reveals an important connection between differential geometry and partial differential equations. The curvature is obtained as the divergence of the unit normal vector field, making it possible to compute geometric quantities directly from image derivatives. This observation is at the heart of geometric active contours and level set methods.

Images as Surfaces

Let us now examine briefly the case of surfaces in $\mathbb{R}^3$. Let D be an open subset of $\mathbb{R}^2$ and let

$$S : D \to \mathbb{R}^3, \qquad (u, v) \mapsto S(u, v),$$

be a regular parametrized surface.

We assume that the vectors S_u and S_v are noncollinear for every $(u, v) \in D$, so that they form a basis of the tangent plane. The unit normal vector to the surface is

$$N(u, v) = \frac{S_u \times S_v}{|S_u \times S_v|}.$$

Some classical notation is as follows:

$$\begin{aligned} E(u, v) &= |S_u|^2, \\ F(u, v) &= S_u \cdot S_v, \\ G(u, v) &= |S_v|^2, \end{aligned}$$

which are the coefficients of the first fundamental form. Similarly,

$$\begin{aligned} L(u, v) &= S_{uu} \cdot N = -S_u \cdot N_u, \\ M(u, v) &= S_{uv} \cdot N = -\tfrac{1}{2}\left(S_u \cdot N_v + S_v \cdot N_u\right), \\ P(u, v) &= S_{vv} \cdot N = S_v \cdot N_v, \end{aligned}$$

which are the coefficients of the second fundamental form. Using this notation, we have

$$|S_u \wedge S_v| = \sqrt{EG - F^2},$$

and the surface element is

$$ds = \sqrt{EG - F^2}\, du\, dv.$$

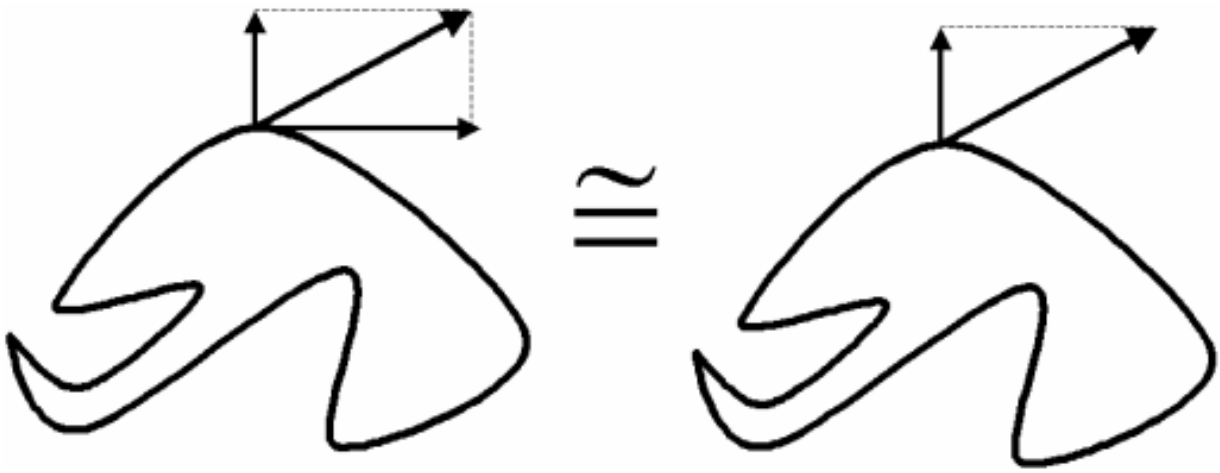


Figure 1.5: Most general form of a curve evolution flow. The velocity is decomposed into its tangential and normal components, the former not affecting the geometry of the flow, just its parameterization.

The mean curvature H can be written as

$$H = \frac{EP + GL - 2FM}{2(EG - F^2)}. \tag{1.7}$$

Curvature Flow

A curve evolution can generally be decomposed into a tangential and a normal component,

$$\frac{\partial C}{\partial t} = V_T T + V_N N.$$

The tangential component only changes the parametrization of the curve and does not modify its geometric shape. Therefore, from a geometric point of view, only the normal component influences the evolution of the interface. For this reason, geometric active contour models are usually written in the form

$$\frac{\partial C}{\partial t} = V_N N.$$

Figure 1.5 illustrates this decomposition.

Among all possible geometric flows, one of the most fundamental is obtained when the normal velocity is chosen equal to the curvature,

$$V_N = \kappa.$$

The evolution law then becomes

$$\frac{\partial C}{\partial t} = \kappa N.$$

This motion is known as curvature flow. Under curvature flow, highly curved regions move faster than flatter regions, producing a smoothing effect on the contour.

Consequently, irregularities and noise are progressively removed while the overall shape is preserved.

Curvature flow plays a central role in geometric image processing and forms one of the main components of Geodesic Active Contour models.

Curvature flow may be viewed as a geometric smoothing process. However, by itself it tends to shrink closed curves and may eventually collapse them to a point. Geodesic Active Contour models overcome this limitation by introducing image-dependent terms that attract the contour towards object boundaries.

Energy Minimization and Curve Evolution

Many active contour models can be interpreted as gradient descent methods for minimizing an energy functional.

Let $E(C)$ be an energy associated with a curve C. The contour evolves according to

$$\frac{\partial C}{\partial t} = -\nabla E(C),$$

where $\nabla E(C)$ denotes the variational derivative of the energy. At equilibrium, $\nabla E(C) = 0$, and the contour reaches a stationary configuration corresponding to a local minimum of the energy.

This variational viewpoint provides the theoretical basis for both classical snakes and Geodesic Active Contour models.

Geometric Quantities in the Level Set Framework

In the level set method, a curve is represented implicitly as the zero level set of a function $\phi(x, y, t)$. The contour is defined by

$$C(t) = \{(x, y) : \phi(x, y, t) = 0\}.$$

Within this framework, the unit normal vector becomes

$$N = \frac{\nabla \phi}{|\nabla \phi|},$$

and the curvature can be expressed as

$$\kappa = \operatorname{div}\left(\frac{\nabla \phi}{|\nabla \phi|}\right).$$

These formulas are of fundamental importance because they allow geometric quantities to be computed directly from the level set function without explicit parameterization of the contour.

This section introduced the main geometric concepts required for the study of active contour models, including tangent and normal vectors, curvature, curve evolution, and curvature-driven

flows. These notions constitute the mathematical foundation of geometric deformable models. In the next chapter, they will be combined with image-dependent metrics to derive the Geodesic Active Contour model and its associated evolution equations.

1.4 Partial Differential Equations

Partial Differential Equations (PDEs) constitute one of the most powerful mathematical tools for modeling dynamic phenomena involving several independent variables. They arise naturally in numerous scientific disciplines, including fluid mechanics, heat transfer, elasticity, electromagnetism, and image processing.

Over the last decades, PDE-based techniques have become increasingly important in computer vision and image analysis. Many fundamental tasks such as image denoising, enhancement, restoration, segmentation, and contour detection can be formulated as the solution of suitable partial differential equations.

In particular, active contour models and level set methods rely heavily on geometric PDEs to describe the evolution of object boundaries. Therefore, a basic understanding of partial differential equations is essential before introducing Geodesic Active Contour models.

Definition of a Partial Differential Equation

A partial differential equation is an equation involving an unknown function and its partial derivatives with respect to several independent variables.

Let $u = u(x_1, x_2, \ldots, x_n)$ be an unknown function defined on a domain $\Omega \subset \mathbb{R}^n$. A general PDE can be written as

$$F\left(x, u, \nabla u, \nabla^2 u, \ldots\right) = 0,$$

where

- $x = (x_1, \ldots, x_n)$ denotes the spatial variables,
- ∇u denotes the gradient of u,
- $\nabla^2 u$ denotes the Hessian matrix,
- F is a given function.

When time is involved, the unknown function is written as $u = u(x, t)$, and the PDE typically describes the temporal evolution of a physical quantity.

The Heat Equation

The heat equation is one of the simplest and most fundamental PDEs. It is given by

$$u_t = \Delta u.$$

In two dimensions,

$$u_t = u_{xx} + u_{yy}.$$

The equation describes the diffusion of heat in a medium.
When interpreted in image processing, the image intensity plays the role of temperature.
The diffusion process smooths intensity variations and reduces noise.
An important property of the heat equation is the maximum principle, which guarantees that no new extrema are created during the evolution.
However, isotropic diffusion tends to blur image edges, which motivates the development of nonlinear diffusion models.

Diffusion Processes in Image Processing

Diffusion can be viewed as a smoothing mechanism that transfers information from regions of high intensity to neighboring regions.
The general diffusion equation can be written as

$$u_t = \operatorname{div}(D\nabla u),$$

where D denotes a diffusion coefficient.
If D is constant, one recovers the classical heat equation.
If D depends on image features, the diffusion process becomes nonlinear and can preserve important structures such as edges.
This observation led to the development of anisotropic diffusion models.

Nonlinear Diffusion Equations

A major breakthrough in PDE-based image processing was the introduction of nonlinear diffusion.
The general form is

$$u_t = \operatorname{div}\left(g(|\nabla u|)\nabla u\right),$$

where $g : \mathbb{R}^+ \to \mathbb{R}^+$ is a decreasing function. A typical choice is $g(s) = \frac{1}{1+\left(\frac{s}{K}\right)^2}$.
In homogeneous regions, $|\nabla u| \approx 0$, and diffusion remains strong. Near edges, $|\nabla u| \gg 0$, which reduces diffusion and preserves boundary information.
This principle forms the foundation of many modern PDE-based image processing techniques.

Hamilton–Jacobi Equations

Another important family of PDEs is the Hamilton–Jacobi equations. Their general form is

$$u_t + H(\nabla u) = 0,$$

where H is called the Hamiltonian. These equations naturally arise in front propagation problems and geometric curve evolution.

A particularly important example is

$$u_t + F|\nabla u| = 0,$$

where F denotes a propagation speed. This equation will reappear in the level set formulation of moving interfaces.

Geometric Partial Differential Equations

Geometric PDEs describe the evolution of shapes and interfaces according to intrinsic geometric quantities.

Consider a family of curves $C(q,t)$. The evolution law can be written as

$$\frac{\partial C}{\partial t} = FN,$$

where

- F is the normal velocity,
- N is the unit normal vector.

If $F = \kappa$, one obtains the curvature flow

$$\frac{\partial C}{\partial t} = \kappa N.$$

Curvature flow smooths the contour by eliminating small irregularities.

Geometric PDEs constitute the mathematical basis of active contour models.

Variational Formulation and Gradient Flows

Many PDEs can be derived from an energy minimization principle.

Let $E(u)$ be an energy functional. The associated gradient flow is

$$u_t = -\frac{\delta E}{\delta u},$$

where $\frac{\delta E}{\delta u}$ denotes the variational derivative of the energy.

The solution evolves in the direction of the steepest descent of the energy until a stationary state is reached.

This variational viewpoint is particularly important in image segmentation because many active contour models are obtained by minimizing geometric energies.

PDEs in Image Segmentation

PDEs provide a natural framework for image segmentation.
They offer several advantages:

- mathematical rigor;
- robustness to noise;
- smooth contour evolution;
- incorporation of geometric constraints;
- compatibility with variational methods.

In active contour models, image boundaries are extracted by evolving a curve according to a PDE that combines image information and geometric regularization.
The resulting evolution equation generally contains two competing mechanisms:

1. an attraction force toward image edges;
2. a smoothing force based on curvature.

The balance between these terms determines the quality of the final segmentation.

1.5 Level Set Method

The level set method is a powerful numerical and mathematical framework for representing and tracking evolving interfaces. It was introduced by Osher and Sethian [12] in the late 1980s and has since become a fundamental tool in computational geometry, fluid dynamics, and image processing.
In the context of image segmentation, the level set method provides a flexible way to represent evolving contours without requiring explicit parameterization. This allows natural handling of complex deformations such as splitting and merging of shapes, which are difficult to manage in classical parametric active contour models.

Implicit Representation of Curves

Let a moving curve be denoted by

$$C(t) \subset \mathbb{R}^2.$$

Instead of representing the curve explicitly, the level set method introduces an auxiliary scalar function

$$\phi : \Omega \times [0, +\infty) \to \mathbb{R},$$

such that the curve is represented as the zero level set:

$$C(t) = \{(x, y) \in \Omega \, : \, \phi(x, y, t) = 0\}.$$

In this formulation:

- $\phi(x, y, t) > 0$ inside the curve,
- $\phi(x, y, t) < 0$ outside the curve,
- $\phi(x, y, t) = 0$ defines the interface.

This implicit representation eliminates the need to explicitly track points along the curve.

Signed Distance Function

A common and convenient initialization of the level set function is the signed distance function defined by

$$\phi(x, y, 0) = \begin{cases} d(x, y, C_0) & \text{inside the curve,} \\ -d(x, y, C_0) & \text{outside the curve,} \end{cases}$$

where $d(x, y, C_0)$ denotes the Euclidean distance from the point (x, y) to the initial contour C_0.
The signed distance function satisfies the important property

$$|\nabla \phi| = 1.$$

This property improves numerical stability and is often preserved through reinitialization procedures.

Geometric Quantities in Level Set Form

One of the main advantages of the level set framework is that geometric quantities can be expressed directly in terms of ϕ.
The unit normal vector to the interface is given by

$$N = \frac{\nabla \phi}{|\nabla \phi|}.$$

The curvature of the level set is expressed as

$$\kappa = \operatorname{div}\left(\frac{\nabla \phi}{|\nabla \phi|}\right).$$

These expressions allow curvature-driven motions to be implemented without explicit curve parameterization.

Evolution of the Level Set Function

Consider a moving curve $C(t)$ evolving with normal velocity F:

$$\frac{\partial C}{\partial t} = FN.$$

In the level set formulation, this evolution is translated into a PDE for ϕ:

$$\phi_t + F|\nabla\phi| = 0.$$

This equation is known as the level set equation or Hamilton–Jacobi type equation.
It describes how the implicit function ϕ evolves so that its zero level set moves with velocity F in the normal direction.

Interpretation of the Level Set Equation

The term $F|\nabla\phi|$ ensures that motion occurs in the normal direction only.
The sign of F determines the direction of motion:

- $F > 0$ leads to outward propagation,
- $F < 0$ leads to inward contraction.

This formulation is independent of parameterization and remains valid even when the topology of the curve changes.

Advantages of the Level Set Method

The level set method offers several important advantages:

- **Topological flexibility:** splitting and merging of curves occur naturally.
- **Numerical stability:** geometric quantities are computed from ϕ.
- **High dimensional extension:** the method extends easily to 3D surfaces.
- **Implicit formulation:** no explicit parameterization is required.

In the next chapter, these concepts will be combined with image-driven energies to derive the Geodesic Active Contour model and its corresponding evolution equation.

Chapter 2

Geodesic Active Contours Model

In this chapter, we study variational and geometric approaches to image segmentation, focusing in particular on the snake model and the geodesic active contour framework. These models aim at the automatic detection of object boundaries by evolving an initial curve toward the desired contours.

This problem naturally raises two fundamental questions: how to represent an evolving contour in a mathematically consistent way, and which criteria can reliably characterize true object boundaries in an image.

A common assumption in edge-based segmentation methods is that object boundaries correspond to sharp variations in the image intensity $I(x)$. As a consequence, the magnitude of the gradient $|\nabla I(x)|$ becomes large in the vicinity of edges. This observation motivates the use of $|\nabla I(x)|$, or more generally nonlinear functions of it, as an edge-detector function guiding the evolution of active contours.

The snake and geodesic active contour models have been extensively studied in the literature and constitute fundamental tools in image analysis and computer vision. Although these frameworks can be formulated in both two and three dimensions, we restrict our presentation to the two-dimensional case for simplicity of exposition.

2.1 The Kass-Witkin-Terzopoulos Snake Model

We begin by describing the Kass–Witkin–Terzopoulos model [7], which is, to the best of our knowledge, one of the earliest approaches in this direction.

Let Γ denote the set of image edges (i.e., the boundaries of objects). We assume that

$$\Gamma = \bigcup_{j \in J} C_j,$$

where J is finite or countable and each C_j is a piecewise C^1 closed curve in $\mathbb{R}^2$.

Let $I : \Omega \subset \mathbb{R}^2 \to \mathbb{R}$ be the image intensity function, where Ω is a bounded domain. We assume that the function

$$x = (x_1, x_2) \mapsto |\nabla I(x_1, x_2)|$$

belongs to $W^{1,\infty}(\Omega)$.



Figure 2.1: Example of edge-detector function. $g(s) = \frac{1}{1+s^2}$ has been chosen for the right-hand image. Noise is reduced, and contours are enhanced. Also note the inversion of colors due to the function g.

To characterize edges by low values rather than large values, we introduce a function

$$g : [0, +\infty) \to (0, +\infty)$$

satisfying the following properties:

- g is continuously differentiable and monotonically decreasing,
- $g(0) = 1$ and $\lim_{s\to+\infty} g(s) = 0$.

The function

$$x \mapsto g\big(|\nabla I(x)|\big)$$

is called an *edge-detector function*. A typical choice is

$$g(s) = \frac{1}{1+s^2}.$$

In Kass et al. [7], boundary detection is achieved by matching a deformable model to an image through energy minimization. Because the contours evolve during the minimization process, they were called *snakes*.

Let C denote the set of closed curves in $\mathbb{R}^2$ defined by

$$C = \big\{c : [a,b] \to \Omega\,;\ c \text{ is piecewise } C^1,\ c(a) = c(b)\big\}.$$

For $c \in C$, the associated energy functional is defined by

$$J(c) = \underbrace{\int_a^b |c'(q)|^2\,dq + \beta\int_a^b |c''(q)|^2\,dq}_{\text{internal energy}} + \underbrace{\lambda\int_a^b g^2\big(|\nabla I(c(q))|\big)\,dq}_{\text{external energy}}, \tag{2.1}$$

where

$$c(q) = \big(c_1(q), c_2(q)\big), \qquad c'(q) = \left(\frac{dc_1}{dq}, \frac{dc_2}{dq}\right), \qquad |c'(q)| = \sqrt{\left(\frac{dc_1}{dq}\right)^2 + \left(\frac{dc_2}{dq}\right)^2}.$$

The same notation is used for c''.

The first two terms, called the *internal energy*, impose a smoothness constraint on the evolving curve. The first-order term makes the curve behave like a membrane, whereas the second-order term makes it behave like a thin plate. Setting $\beta = 0$ allows the presence of corners and second-order discontinuities.

The third term, called the *external energy*, attracts the curve toward the object boundaries.

We consider variations of the form

$$c_\varepsilon = c + \varepsilon\eta, \quad \eta(a) = \eta(b) = 0.$$

The first variation of J is computed as follows.

For the first term,

$$\frac{d}{d\varepsilon}\int_a^b |c'_\varepsilon|^2 dq\Big|_{\varepsilon=0} = 2\int_a^b \langle c', \eta'\rangle dq = -2\int_a^b \langle c'', \eta\rangle dq.$$

For the second term,

$$\frac{d}{d\varepsilon}\int_a^b |c''_\varepsilon|^2 dq\Big|_{\varepsilon=0} = 2\int_a^b \langle c'', \eta''\rangle dq = 2\int_a^b \langle c^{(iv)}, \eta\rangle dq.$$

For the external energy,

$$\frac{d}{d\varepsilon}\int_a^b F(c_\varepsilon(q)) dq\Big|_{\varepsilon=0} = \int_a^b \langle \nabla F(c), \eta\rangle dq.$$

Hence, the first variation is

$$\delta J(c)[\eta] = \int_a^b \langle -2c'' + 2\beta c^{(iv)} + \lambda \nabla F(c), \eta\rangle dq.$$

Since this must vanish for all admissible η, we obtain the Euler–Lagrange equation:

$$\begin{cases} -c'' + \beta c^{(4)} + \lambda \nabla F(c) = 0, \\ c(a) = c(b), \end{cases} \tag{2.2}$$

where $c^{(iv)}$ denotes the fourth-order derivative and $F(c_1, c_2) = g^2\big(|\nabla I(c_1, c_2)|\big)$.

Appropriate boundary conditions (such as periodic or clamped conditions) may also be imposed. Since the functional $J(c)$ is nonconvex, uniqueness of solutions cannot be guaranteed. Consequently, solving (2.2) generally leads only to a local minimizer, as originally observed in Kass et al. [7].

The main idea of this approach is therefore to reformulate contour detection as an energy minimization problem.

However, this model suffers from several important drawbacks:

- The functional $J(c)$ is not intrinsic because it depends on the parametrization of the curve c. Different parametrizations of the same geometric curve may lead to different solutions.

- Due to the regularity constraints, the model cannot naturally handle topological changes. In particular, it is difficult to detect multiple objects simultaneously, and the model has difficulties in detecting highly nonconvex objects.

- In practice, the numerical resolution of (2.2) is achieved by introducing an artificial time parameter $t \geq 0$ and considering the dynamical system

$$\begin{cases} \dfrac{\partial c}{\partial t}(t,q) = -c''(t,q) + \beta c^{(iv)}(t,q) + \lambda \nabla F(c(t,q)), \\ c(0,q) = c_0(q), \\ c(t,a) = c(t,b), \end{cases} \tag{2.3}$$

  where $c_0(q)$ is an initial curve surrounding the object to be detected.

  Several numerical difficulties arise when solving (2.3). Since the evolution converges only toward a local minimum, the initial curve $c_0(q)$ must be chosen sufficiently close to the desired object boundary.

  Another major difficulty lies in the selection and evolution of the marker points used to discretize the parametrized curve. Their positions must be updated continuously according to the numerical approximation of the motion equations. During large and complex deformations, several problems may occur. For instance, marker points may become excessively concentrated in some regions or too sparse in others, leading to numerical instabilities and inaccurate detections.

We now show how these difficulties can be overcome by the geodesic active contour model.

2.2 The Geodesic Active Contours Model

2.2.1 Geometric Motivation

The main limitation of classical snake models is that they are formulated in terms of a parametrized curve. Consequently, the resulting energy depends on the chosen parametrization and does not naturally handle topological changes such as merging or splitting contours.
To overcome these difficulties, Caselles, Kimmel, and Sapiro [4] proposed a geometric formulation of active contours. Their fundamental idea is to regard object boundaries as geodesics in a Riemannian space whose metric is induced by the image itself.
Let $g(|\nabla I|)$ be an edge indicator function satisfying

$$g(|\nabla I|) \approx 1 \quad \text{in homogeneous regions,}$$

and

$$g(|\nabla I|) \approx 0 \quad \text{near object boundaries.}$$

Using this function, the Euclidean metric $ds^2 = dx^2 + dy^2$ is replaced by the image-dependent metric

$$g^2(|\nabla I|)\left(dx^2 + dy^2\right).$$

Under this new metric, the length of a curve (c) becomes

$$\int g(|\nabla I(c(q))|)|c'(q)|, dq.$$

Since the edge detector assumes very small values near object boundaries, curves lying on image edges become geodesics of minimal weighted length. Consequently, boundary detection can be reformulated as the search for geodesics in the Riemannian manifold induced by the image.

This geometric interpretation constitutes the foundation of the Geodesic Active Contour (GAC) model and explains the appearance of the weighted length functional introduced below.

In the Kass et al. model (2.1), the term $\beta \int_a^b |c''(q)|^2 dq$ (the elasticity term) is a second- order smoothness component that minimizes the squared curvature. As we will see later, the model with $\beta = 0$ also decreases the curvature, making this term redundant. This observation motivates the introduction of the simplified functional J_1 defined by

$$J_1(c) = \int_a^b |c'(q)|^2 dq + \lambda \int_a^b g^2(|\nabla I(c(q))|) dq \tag{2.4}$$

on the set $C = \{c : [a,b] \to \Omega, c \text{ piecewise } C^1, c(a) = c(b)\}$. Still, the functional J_1 is not yet satisfactory, because it is not intrinsic; that is, it depends on the parametrization of c. So the idea is to introduce the functional J_2 defined by [4]

$$J_2(c) = 2\sqrt{\lambda} \int_a^b g(|\nabla I(c(q))|)|c'(q)| dq. \tag{2.5}$$

It is easy to see that J_2 is now intrinsic: If we define a new parametrization of the curve via $q = \varphi(r)$, $\varphi : [a', b'] \to [a, b]$, $\varphi' > 0$, we obtain

$$J_2(c) = 2\sqrt{\lambda} \int_{a'}^{b'} g(|\nabla I(\bar{c}(r))|)|\bar{c}'(r)| dr$$

with $\bar{c}(r) = c(\varphi(r))$, i.e., there is no change in the energy. Therefore, if we compare J_2 to the classical length definition of a curve $\left(L = \int_a^b \left|c'(q)\right| dq\right)$, we observe that J_2 can be seen as a new length by weighting the Euclidean length. The weight is $g(|\nabla I(c(q))|)$, which contains information regarding the objects' boundaries. In other words, we have defined a new metric (a Riemannian metric) for which the object boundaries are sought as geodesics of the induced Riemannian metric. Beyond this geometric argument, we will see that this formulation also enables us to apply very efficient numerical schemes.

Starting from J_1, we have introduced a functional J_2 that is intrinsic and that can be interpreted as a weighted Euclidean length. Now the question is to understand the link between the two minimization problems.

In [4], Caselles et al. have shown, by using concepts of Hamiltonian theory, that minimizing J_1 is "equivalent" to minimizing J_2. This idea has been widely reused in the sequel to justify this choice. However, it is unsatisfactory in two ways. The first is that the notion of equivalence is not even clear. It would be natural to say that two minimization problems are equivalent if they have the same solutions or possibly if they have the same extremals. In our case we cannot apply these notions, since it is not clear whether the problem $\inf_c J_2(c)$ has a solution or not. The edge function g being degenerate in any neighborhood of an edge, it would be difficult to bound minimizing sequences in any reasonable space. The second is that we may wonder why it is necessary to use concepts from Hamiltonian theory and whether it could be possible instead to use classical techniques of the calculus of variations.

In this direction, Aubert and Blanc-Féraud [2] defined a precise notion of equivalence and proved it in this context. We do not reproduce the whole discussion of [2], but we will state only what can be, in our opinion, a correct definition of equivalence. Before formulating that definition we need to study the variations of the energies in a neighborhood of a given curve $c(q)$. Calculations developed below are presented in detail, since they will be useful afterwards.

Let $c(q) \in C$ and let $c(t,q)$ be a family of curves, where $t \geq 0$ is an exterior parameter (the time) such that $c(0,q) = c(q)$. Let us set $J_i(t) = J_i(c(t,q))$, $i = 1,2$. The first step consists in computing $J_i'(t)$, $i = 1,2$.

- **Calculus of $J_1'(t)$.** We have

$$J_1(c) = \int_a^b \left\| \frac{\partial c}{\partial q}(t,q) \right\|^2 dq + \lambda \int_a^b g^2(|\nabla I(c(t,q))|) dq.$$

  In order to simplify the notations we write c instead of $c(t,q)$, g for $g(|\nabla I(c(t,q))|)$, and we suppose that $\lambda = 1$. We will also write $u \cdot v = \langle u, v \rangle$. Thus

$$\frac{1}{2} J_1'(t) = \int_a^b \left\langle \frac{\partial c}{\partial q}, \frac{\partial^2 c}{\partial t \partial q} \right\rangle dq + \int_a^b \left\langle \frac{\partial c}{\partial t}, g \nabla g \right\rangle dq.$$

  By integrating the first integral by parts with respect to q (we assume that $c(t,a) = c(t,b)$ and $\frac{\partial c}{\partial q}(a,t) = \frac{\partial c}{\partial q}(t,b)$ for all $t > 0$) we get

$$\frac{1}{2} J_1'(t) = \int_a^b \left\langle \frac{\partial c}{\partial t}, -\frac{\partial^2 c}{\partial q^2} + g \nabla g \right\rangle dq.$$

  Denoting the arc length by $s = s(q) = \int_a^q \left\| \frac{\partial c}{\partial \tau}(\tau) \right\| d\tau$, we always have for any curve c,

$$\frac{\partial^2 c}{\partial q^2} = \left\| \frac{\partial c}{\partial q} \right\|^2 \frac{\partial^2 c}{\partial s^2} + \left\langle T, \frac{\partial^2 c}{\partial q^2} \right\rangle T,$$

  where T denotes the unit tangent vector: $T = \frac{\partial c}{\partial q} / \left\| \frac{\partial c}{\partial q} \right\|$. Let N be the unit normal vector to the curve and let κ be the curvature. Then we have

$$\frac{\partial^2 c}{\partial s^2} = \kappa N.$$

Thus $J_1'(t)$ becomes

$$\frac{1}{2}J_1'(t) = \int_a^b \left\langle \frac{\partial c}{\partial t}, -\kappa \left\| \frac{\partial c}{\partial q} \right\|^2 N - \left\langle T, \frac{\partial^2 c}{\partial q^2} \right\rangle T + g\nabla g \right\rangle dq.$$

If we decompose the vector ∇g in the tangential and normal directions

$$\nabla g = \langle \nabla g, N\rangle N + \langle \nabla g, T\rangle T,$$

we obtain

$$\frac{1}{2}J_1'(t) = \int_a^b \left\langle \frac{\partial c}{\partial t}, \left(-\kappa \left\| \frac{\partial c}{\partial q} \right\|^2 + \langle g\nabla g, N\rangle\right) N + \left(\langle g\nabla g, T\rangle - \left\langle T, \frac{\partial^2 c}{\partial q^2} \right\rangle\right) T \right\rangle dq.$$

Therefore, thanks to the Cauchy-Schwarz inequality the flow for which $J_1(t)$ decreases most rapidly is given by

$$\frac{\partial c}{\partial t} = \left(\kappa \left\| \frac{\partial c}{\partial q} \right\|^2 - \langle g\nabla g, N\rangle\right) N - \left(\langle g\nabla g, T\rangle - \left\langle T, \frac{\partial^2 c}{\partial q^2} \right\rangle\right) T. \tag{2.6}$$

- **Calculus of $J_2'(t)$.** We have

$$\frac{1}{2}J_2(t) = \int_a^b g(|\nabla I(c(t,q))|) \left\| \frac{\partial c}{\partial q}(t,q) \right\| dq. \tag{2.7}$$

Then

$$\frac{1}{2}J_2'(t) = \int_a^b g \left\langle \frac{(\partial c/\partial q)}{\|\partial c/\partial q\|}, \frac{\partial^2 c}{\partial t \partial q} \right\rangle dq + \int_a^b \left\| \frac{\partial c}{\partial q} \right\| \langle \nabla g, \frac{\partial c}{\partial t}\rangle dq.$$

The first integral on the right-hand side is integrated by parts with respect to q:

$$\frac{1}{2}J_2'(t) = -\int_a^b \left[\left\langle g \frac{\partial}{\partial q}\left(\frac{\partial c/\partial q}{\|\partial c/\partial q\|}\right) + \frac{\partial c/\partial q}{\|\partial c/\partial q\|}\langle \nabla g, \frac{\partial c}{\partial q}\rangle, \frac{\partial c}{\partial t} \right\rangle \right] dq + \int_a^b \left\| \frac{\partial c}{\partial q} \right\| \langle \nabla g, \frac{\partial c}{\partial t}\rangle dq.$$

This equation can be rewritten as

$$\frac{1}{2}J_2'(t) = \int_a^b \left\| \frac{\partial c}{\partial q} \right\| \left\langle \frac{\partial c}{\partial t}, \nabla g - \frac{1}{\|\partial c/\partial q\|}\frac{\partial}{\partial q}\left(\frac{\partial c/\partial q}{\|\partial c/\partial q\|}\right) g - \frac{\partial c/\partial q}{\|\partial c/\partial q\|}\left\langle \nabla g, \frac{\partial c/\partial q}{\|\partial c/\partial q\|} \right\rangle \right\rangle dq,$$

and recalling the definitions of T, N, and κ, we get

$$\frac{1}{2}J_2'(t) = \int_a^b \left\| \frac{\partial c}{\partial q} \right\| \left\langle \frac{\partial c}{\partial t}, \nabla g - \kappa g N - \langle T, \nabla g\rangle T \right\rangle dq.$$

Again decomposing ∇g on the basis (N, T), we finally obtain

$$\frac{1}{2}J_2'(t) = \int_a^b \left\| \frac{\partial c}{\partial q} \right\| \left\langle \frac{\partial c}{\partial t}, \langle \nabla g, N\rangle N - \kappa g N \right\rangle dq, \tag{2.8}$$

so the direction for which $J_2(t)$ decreases most rapidly is given by

$$\frac{\partial c}{\partial t} = (\kappa g - \langle \nabla g, N\rangle) N. \tag{2.9}$$

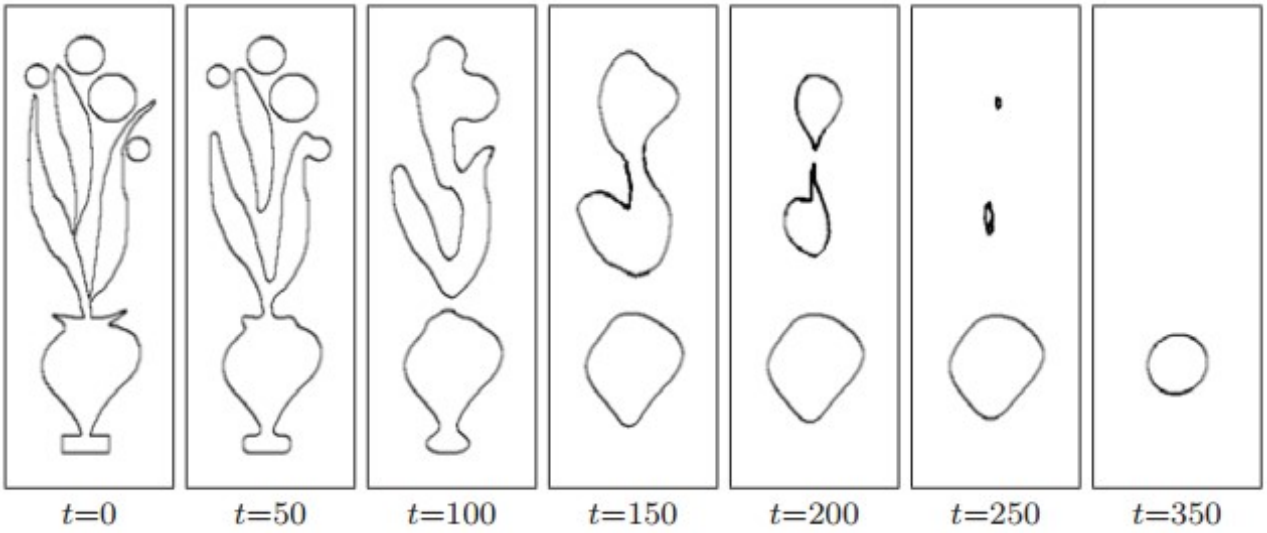


Figure 2.2: Example of the mean curvature motion.

Remark Note that if $g \equiv 1$, then the flow (2.9) reduces to

$$\frac{\partial c}{\partial t} = \kappa N, \tag{2.10}$$

which is the well-known mean curvature motion (or shortening flow). This flow decreases the total curvature as well as the number of zero crossings and the value of maxima/minima curvature. Therefore, it has the properties of shortening (an initial curve shrinks under (2.10) to a point in finite time with asymptotically circular shape) as well as smoothing (points with high curvature evolve faster and disappear asymptotically). An example is shown in Figure 2.2. We are now in position to state what we mean by saying that the two minimization problems $\inf_c J_1(c)$ and $\inf_c J_2(c)$ are equivalent.

Definition 2.2.1. ***(equivalence between*** $\inf_c J_1(c)$ ***and*** $\inf_c J_2(c)$***)***
The problems $\inf_c J_1(c)$ *and* $\inf_c J_2(c)$ *are equivalent if for any curve* $c \in C$ *there exists a neighborhood* $V(c)$ *of* c *such that in* $V(c)$ *the flow that most decreases* J_1 *is also a decreasing flow for* J_2 *and vice versa.*

In order to apply this criterion, we need a more precise definition of an edge.

Definition 2.2.2. ***(edge)***
Let $c \in C$*. We say that* c *is an edge of the image* I *if there exists* ε_0 *such that* $\forall \varepsilon < \varepsilon_0$, $\exists \alpha_\varepsilon$, $\lim_{\varepsilon \to 0} \alpha_\varepsilon = 0$, *such that* $|\nabla I(x)| \geq 1/\varepsilon$ *if* $x \in V_\varepsilon = \{x : d(x;c) \leq \alpha_\varepsilon\}$, *where* d *is the distance function.*

Theorem 2.2.1. *Let us assume that the edge-detection function* g *satisfies the following: For any edge* $c \in C$ *there exist* $l, l' \in \mathbb{Q}$, $l < l'$, *such that* $\forall \varepsilon < \varepsilon_0$, $\forall x \in V_\varepsilon$*:*

(i) $g(|\nabla I(x)|) = O(\varepsilon^l)$.

(ii) $|\nabla g(|\nabla I(x)|)| = O(\varepsilon^{l'})$.

Then the two minimization problems $\inf_c J_1(c)$ *and* $\inf_c J_2(c)$ *are equivalent in the sense of Definition 2.2.1.*

Proof We have to prove that the flow (2.6) that makes J_1 decrease most rapidly also makes J_2 decrease, and conversely, the flow (2.9) that makes J_2 decrease most rapidly also makes J_1 decrease. In order to do that we replace $\partial c/\partial t$ given by (2.6) in the expression of $J_2'(t)$ and vice versa.
When $\partial c/\partial t$ is given by (2.6), $J_2'(t)$ becomes

$$J_2'(t) = \int_a^b -g(\langle \nabla g, N\rangle - \kappa g)\left(\langle \nabla g, N\rangle - \kappa g\left\|\frac{\partial c}{\partial q}\right\|^2\right)\left\|\frac{\partial c}{\partial q}\right\| dq. \tag{2.11}$$

In the same way, if we replace $\partial c/\partial t$ by its expression in (2.9), then $J_1'(t)$ becomes

$$J_1'(t) = \int_a^b -g(\langle \nabla g, N\rangle - \kappa g)\left(\langle \nabla g, N\rangle - \kappa g\left\|\frac{\partial c}{\partial q}\right\|^2\right)\left\|\frac{\partial c}{\partial q}\right\| dq. \tag{2.12}$$

In order to determine the sign of $J_2'(t)$ in (2.11) or the sign of $J_1'(t)$ in (2.12) it suffices to study a.e. q the sign of the integrand

$$z(t,q) = -g(\langle \nabla g, N\rangle - \kappa g)\left(\langle \nabla g, N\rangle - \kappa g\left\|\frac{\partial c}{\partial q}\right\|^2\right).$$

By developing this expression we obtain:

$$z(t,q) = -\kappa^2\left\|\frac{\partial c}{\partial q}\right\|^2 g + \kappa\left(\left\|\frac{\partial c}{\partial q}\right\|^2 + g^2\right)\langle \nabla g, N\rangle - g(\langle \nabla g, N\rangle)^2.$$

Let us recall now that g stands for $g(|\nabla I(c(t,q))|)$ and let us assume that $c(t,q)$ is in a neighborhood V_ε of an edge $c(0,q)$ of the image I. Then we have, thanks to the assumptions (i) and (ii) on g

$$z(t,q) \approx -a\varepsilon^l \pm b\varepsilon^{l'} - c\varepsilon^{2l'}$$

with $a, b, c \geq 0$. When ε is small enough the sign of $z(t,q)$ is given by the sign of $-a\varepsilon^l$, and so it is negative (we suppose that κ is bounded; otherwise, as soon as $|\kappa| \gg 1$ we have $\kappa^2 \geq |\kappa|$, and z would remain nonpositive). ■

The Caselles et al. model [4] may be improved by adding to the right-hand side of (2.9) a supplementary term

$$\frac{\partial c}{\partial t} = (\kappa g - \langle \nabla g, N\rangle + \alpha g)N. \tag{2.13}$$

The main interest in adding αg to the velocity is that it makes the detection of nonconvex objects easier and it increases the speed of convergence. In fact, $\alpha \geq 0$ must be chosen large enough so that the coefficient $(\kappa + \alpha)$ remains of constant sign. Consequently, the curvature κ can have a nonconstant sign, and nonconvex shapes can then be detected.

Remark It is worth noting that equation (2.13) does not come from any energy unless the function g is a constant (and this is not the case, since g is a detector function). As a matter of fact, the flow $\partial c/\partial t = \alpha N$ with $\alpha \geq 0$ (a constant) is the flow deduced from the area energy

$$A(t) = -\frac{1}{2}\int_a^b \left\langle c(t,q), \left(-\frac{\partial c_2}{\partial q}, \frac{\partial c_1}{\partial q}\right)\right\rangle dq.$$

For each $t > 0$, $A(t)$ is the area enclosed by $c(t,q) = (c_1(t,q), c_2(t,q))$, and it is easy to verify that

$$A'(t) = -\int_a^b \left\langle \frac{\partial c}{\partial t}, N\right\rangle \left\|\frac{\partial c}{\partial q}\right\| dq.$$

Thus the direction in which $A(t)$ is decreasing most rapidly is $\partial c/\partial t = N$. ■

To summarize the situation, starting from the initial formulation of Kass et al. (2.1), we introduced the energy J_1 and an intrinsic (geometric) functional J_2. We clearly defined the link between these two optimization problems. From a numerical point of view, we can wonder which formulation is the best to choose. As we are going to see in the next section, the Euler-Lagrange equations associated with J_2 can be written in an Eulerian formulation by using a level set approach (which is not the case for J_1). The level set approach is based on the description of the curve as the zero crossing of a higher-dimensional function and allows major simplifications.

2.2.2 Interpretation of the Geodesic Flow

The evolution equation

$$(\kappa g - \langle \nabla g, N\rangle)N \tag{2.14}$$

constitutes the fundamental motion law of the Geodesic Active Contour model. In contrast with the classical snake formulation, this evolution has a clear geometric interpretation and can be viewed as the combination of two distinct forces acting on the evolving contour.

To better understand the behavior of the model, let us examine separately the two terms appearing in (2.14).

Curvature Regularization Term

The first contribution, g,κ,N is a curvature-driven smoothing force.

Recall that κ denotes the curvature of the contour and N its inward unit normal vector. When the edge-detector function satisfies $g \equiv 1$, equation (2.14) reduces to κN which is the classical mean curvature motion.

This motion tends to shorten the contour and eliminate oscillations. Regions of high curvature evolve more rapidly than flatter regions, producing a regularization effect that progressively smooths the contour. Consequently, small irregularities and spurious structures generated by image noise are naturally removed during the evolution.

The multiplication by the factor g modulates this smoothing effect. Near object boundaries, where g becomes small, the curvature motion slows down considerably, preventing excessive smoothing of the detected contours.

Attraction Toward Image Edges

The second contribution, $-\langle \nabla g, N \rangle N$ acts as an attraction force toward image boundaries.
Since the edge-detector function is designed to decrease sharply near strong image gradients, its gradient vector ∇g points toward regions where the image gradient varies significantly. The quantity $\langle \nabla g, N \rangle$ measures the component of this variation in the normal direction of the contour.
When the contour is far from an edge, the value of ∇g is generally nonzero and the force $-\langle \nabla g, N \rangle N$ drives the curve toward locations where the edge-detector function reaches its minimum values. These locations correspond to object boundaries.
As the contour approaches an edge, the attraction force progressively balances the smoothing effect produced by the curvature term, leading to a stationary configuration.

Competition Between Smoothing and Attraction

The evolution of the contour results from the competition between the two mechanisms described above.
The curvature term $g\kappa N$ promotes regularity and prevents the formation of irregular shapes, whereas the advection term $-\langle \nabla g, N \rangle N$ attracts the contour toward image edges.
This balance is one of the main strengths of the Geodesic Active Contour model. The contour remains smooth while simultaneously being guided by image information.
At equilibrium, the normal velocity vanishes:

$$g\kappa - \langle \nabla g, N \rangle = 0.$$

The detected contour therefore corresponds to a curve for which the geometric smoothing effect is exactly balanced by the attraction generated by the image gradients.

Effect of the Balloon Force

In practical applications, the modified evolution

$$(\kappa g - \langle \nabla g, N \rangle + \alpha g) N$$

is often preferred.
The additional term $\alpha g N$ is known as the *balloon force* or *inflation force*. It acts as a pressure term that pushes the contour outward when $\alpha > 0$ or inward when $\alpha < 0$.

The balloon force increases the capture range of the model and facilitates the detection of highly nonconvex objects. It also accelerates the convergence of the contour toward the desired boundary, especially when the initial contour is placed far from the target object.
Consequently, the complete Geodesic Active Contour model combines three complementary mechanisms:

- curvature regularization,
- attraction toward image edges,
- balloon-driven propagation.

Together, these mechanisms provide a robust framework for boundary detection and constitute the basis of most modern geometric active contour methods.

2.3 The Level-Set Method

The aim of this section is to find an efficient algorithm to solve (2.13). Naturally, one could parametrize the curve c and discretize the equation, but this direct approach faces difficulties that we will emphasize later. More generally, we are interested in flows governed by equations of the form

$$\begin{cases} \frac{\partial c}{\partial t} = FN, \\ c(0,q) = c_0(q). \end{cases} \tag{2.15}$$

Equation (2.15) says that the curve $c(t,q)$ moves along its normal with a speed F, which may depend on t, c, c', c''. The level set formulation is based on the following observation due to [5, 12]:
A curve can be seen as the zero-level of a function in higher dimension.
For example, a curve in $\mathbb{R}^2$ can be represented as the zero-level line of a function $\mathbb{R}^2 \to \mathbb{R}$ (see Figure 2.3). More precisely, let us suppose that there exists a function $u : \mathbb{R}^+ \times \mathbb{R}^2 \to \mathbb{R}$ such that

$$u(t, c(t,q)) = 0 \quad \forall q, \forall t \geq 0. \tag{2.16}$$

Then if u is sufficiently regular, by differentiating (2.16) with respect to t we obtain

$$\frac{\partial u}{\partial t} + \left\langle \nabla u, \frac{\partial c}{\partial t} \right\rangle = 0,$$

and by replacing the expression for the speed given in (2.15) we get

$$\frac{\partial u}{\partial t} + \langle \nabla u, FN \rangle = 0. \tag{2.17}$$

But recalling that the unit inward normal to the front defined by (2.16) is given by $N = -\frac{\nabla u}{|\nabla u|}$ (we suppose that u is negative inside the curve and positive outside), then (2.17) can be rewritten as

$$\frac{\partial u}{\partial t}(t, c(t,q)) = F|\nabla u(t, c(t,q))|. \tag{2.18}$$

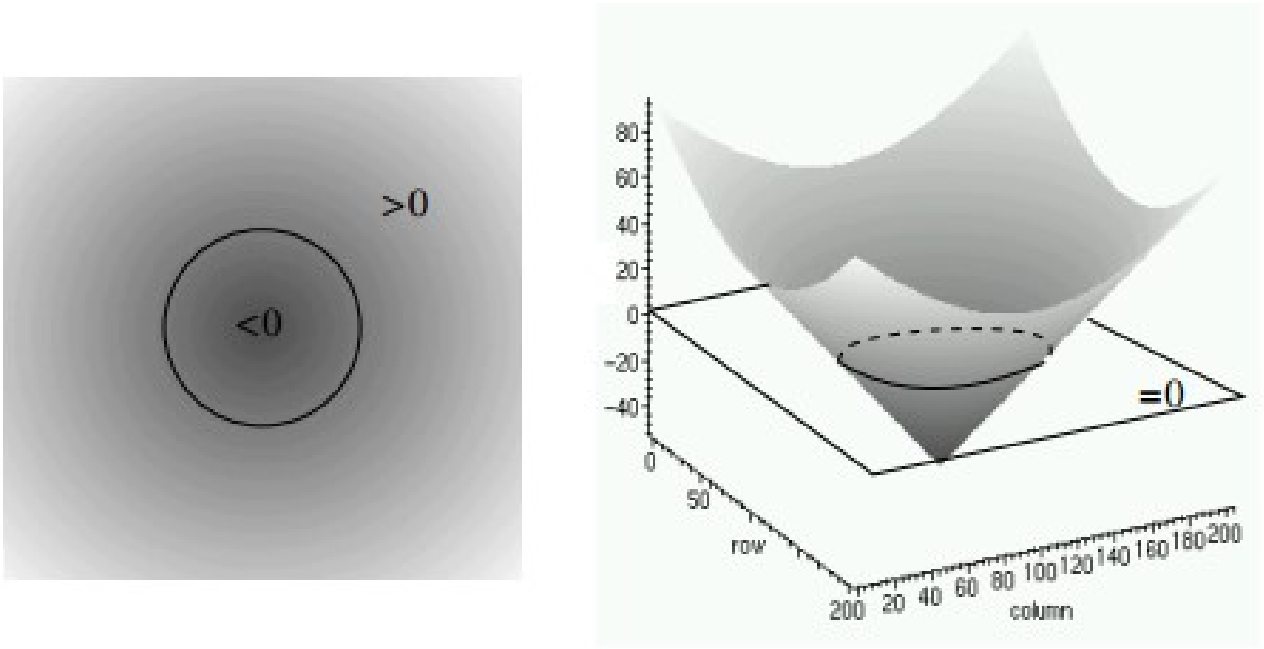


Figure 2.3: Basis of the level set approach: A closed curve can be seen as the zero-level of a function in higher dimension. For instance, the function can be the signed distance to the curve, negative inside and positive outside.

According to the way we have established (2.18), this equation is a priori valid only for the zero-level set of u. But one of the advantages of the method is that u may be regarded as defined on the whole domain $\mathbb{R}^+ \times \Omega$. So, we can solve the PDE

$$\frac{\partial u}{\partial t}(t,x) = F|\nabla u(t,x)|$$

for $t \geq 0$ and $x \in \Omega$ as soon as F is well-defined off the front, i.e., on the whole space. Then once u is calculated on $\mathbb{R}^+ \times \Omega$ we just need to extract the zero-level set of u to get the curve. We will return to this question later.

Of course, we have to add the following conditions.

(i) A boundary condition: One generally chooses that the normal derivative vanishes on $\partial\Omega$ i.e.,

$$\frac{\partial u}{\partial N} = 0 \text{ on } \partial\Omega.$$

(ii) An initial condition at $t = 0$. A good candidate is the signed distance function to an initial given curve $c_0(q)$ surrounding the objects:

$$u(0,x) = \bar{d}(x,c_0) = \begin{cases} +d(x,c_0) & \text{if } x \text{ is outside } c_0, \\ -d(x,c_0) & \text{if } x \text{ is inside } c_0, \end{cases}$$

where $d(x,c_0)$ is the Euclidean distance to c_0.

Therefore, the final model is

$$\begin{cases} \frac{\partial u}{\partial t}(t,x) = F|\nabla u(t,x)| & \text{for } (t,x) \in]0,+\infty[\times\Omega, \\ u(0,x) = \bar{d}(x,c_0), & \\ \frac{\partial u}{\partial N} = 0 & \text{for } (t,x) \in]0,+\infty[\times\partial\Omega. \end{cases} \tag{2.19}$$

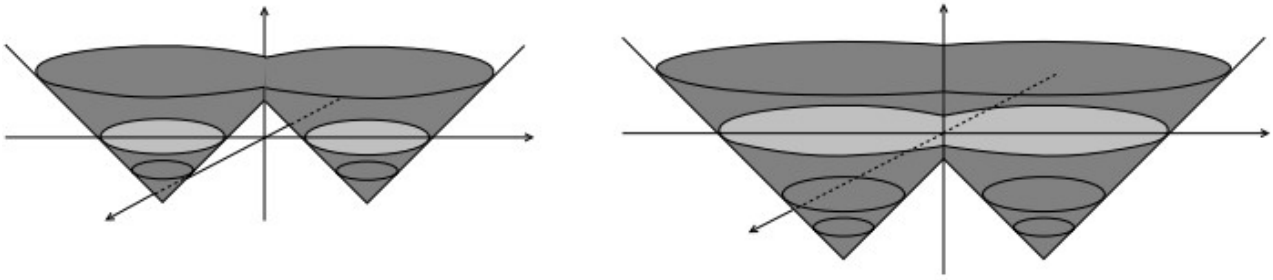


Figure 2.4: Illustration of the change of topology.

The equation (2.19) is called a Hamilton-Jacobi equation. There are many advantages to working with this Eulerian formulation:

- The first is that the evolving function $u(t,x)$ always remains a function as long as F is smooth. But if we consider only the level set $u=0$ (and so the front $c(t,q)$), it may change topology, break, merge as u evolves. We illustrate this in Figure 2.4. This is a main advantage of this representation, since we do not need to take these topological changes into account numerically.

- A second important interest concerns the numerical approximation: We can use a fixed discrete grid in the spatial domain and choose finite-difference approximations for the spatial and temporal derivatives.

- Another advantage is that intrinsic geometric elements of the front such as the normal vector and the curvature can be easily expressed with respect to u. Notice that this is a necessary condition for any representation to be useful.

- Finally, this above level set formulation can be extended and applied in any dimension. For instance, a surface can be represented implicitly by the zero-level set of a function defined in a volume.

This representation is useful as soon as the evolution of a hypersurface is involved and when the motion can be expressed as a velocity along the normal.
This approach has been extensively used in computer vision as well as in other domains. To know more about the level set method: [14, 13].
In image analysis, [3, 4, 8, 9, 11] are some of the papers that first appeared in this direction. All these papers rely on the same ideas. The major difference between them is that [4, 8, 9] start from an energy concept (the minimization of the weighted length), while [3, 11] formulate directly their problem in terms of level sets.

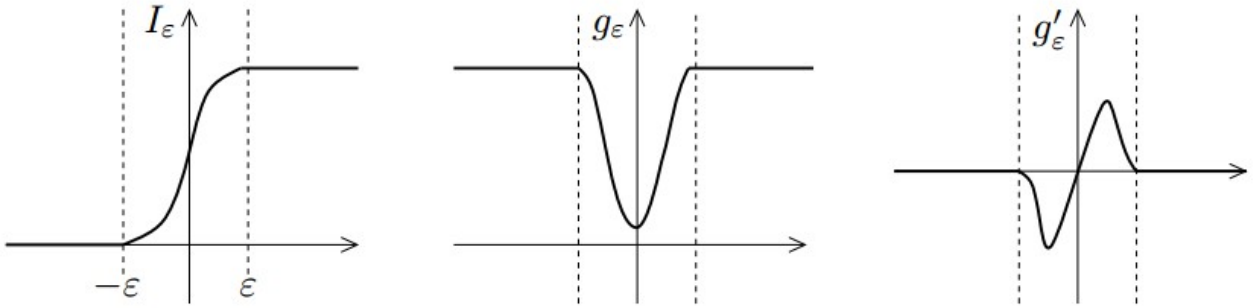


Figure 2.5: The initial signal I_ε and the functions $g_\varepsilon(x)$, $g'_\varepsilon(x)$.

To give an example, let us return to the segmentation problem. We can show that the level sets expression of (2.13) is

$$\frac{\partial u}{\partial t} = \left((\kappa + \alpha)g + \left\langle \nabla g, \frac{\nabla u}{|\nabla u|} \right\rangle\right)|\nabla u|,$$

or, remembering that the curvature κ is given by $\kappa = \operatorname{div}\left(\frac{\nabla u}{|\nabla u|}\right)$,

$$\frac{\partial u}{\partial t} = g(|\nabla I|)\left(\operatorname{div}\left(\frac{\nabla u}{|\nabla u|}\right) + \alpha\right)|\nabla u| + \langle \nabla g, \nabla u\rangle, \tag{2.20}$$

with the boundary and initial conditions of (2.19). In the first term, the coefficient $g(|\nabla I|)$ permits one to stop the evolving curve when it arrives at the object boundaries. The action of the second term, $\langle \nabla g, \nabla u\rangle$, is less obvious. To better understand its contribution, let us consider the following one-dimensional example. Let $I(x)$ be the Heaviside function, $I(x) = 1$ if $x \geq 0$ and $I(x) = 0$ otherwise, and let I_ε be a regularization of I by a cubic function:

$$I_\varepsilon(x) = \begin{cases} 1 & \text{if } x \geq \varepsilon, \\ -\frac{x^3}{4\varepsilon^3} + \frac{3x}{4\varepsilon} + \frac{1}{2} & \text{if } -\varepsilon \leq x \leq \varepsilon, \\ 0 & \text{if } x \leq -\varepsilon. \end{cases}$$

Then, if we set $g_\varepsilon(x) = \frac{1}{1+|I'_\varepsilon(x)|^2}$, it is easy to verify that in a neighborhood of $x = 0$ we have $g_\varepsilon(x) \approx \varepsilon^2$ and $g'_\varepsilon(x) \approx \frac{9}{4\varepsilon^4}x$ (see Figure 2.5). Therefore, the leading term in (2.20) is (in this one-dimensional case) the transport term $g'_\varepsilon(x)u'(x)$. Thus, the front evolves from right to left for $x > 0$ and from left to right for $x < 0$. The point $x = 0$ (the discontinuity front) can be seen as an attractive point. This effect is the same for images.

Note: The term $\langle \nabla g, \nabla u\rangle$ increases the attraction of the deforming contour toward the boundary of objects.

Before proceeding with the approximation we now present results regarding the existence and uniqueness of a solution for (2.20), using the theory of viscosity solutions.

According to the identity

$$\operatorname{div}\left(\frac{\nabla u}{|\nabla u|}\right) = \frac{1}{|\nabla u|^3}\left(u_{x_1}^2 u_{x_2x_2} + u_{x_2}^2 u_{x_1x_1} - 2u_{x_1}u_{x_2}u_{x_1x_2}\right),$$

where $u_{x_i} = \frac{\partial u}{\partial x_i}$, the equation (2.20) can be rewritten as

$$\frac{\partial u}{\partial t} = g(x) \sum_{i,j=1}^{2} a_{i,j}(\nabla u) u_{x_i x_j} + H(x, \nabla u), \tag{2.21}$$

where

$$a_{i,j}(p) = \delta_{i,j} - \frac{p_i p_j}{|p|^2} \quad \text{if } p \neq 0 \quad (\delta_{i,j} \text{ is the Kronecker symbol}), \tag{2.22}$$

$$H(x,p) = \alpha g(x)|p| + \sum_{i=1}^{2} \frac{\partial g}{\partial x_i}(x) p_i \quad \text{with } g(x) = g(|\nabla I(x)|). \tag{2.23}$$

To avoid some tedious technicalities at corners, instead of the Neumann boundary condition $\frac{\partial u}{\partial N} = 0$ on $]0, +\infty[\times\partial\Omega$, we will work with periodic solutions. Of course, we also suppose that the initial condition $u(0,x) = u_0(x)$ is periodic.

Let us recall the definition of viscosity solutions for the parabolic equation (2.21):

Definition 2.3.1. ***(viscosity subsolution, supersolution, solution)***

Let u be in $C([0,T]\times\mathbb{R}^2)$, $0 < T < \infty$. Then u is a viscosity subsolution of (2.21) if for $\phi \in C^2([0,T]\times\mathbb{R}^2)$ the following condition holds: At any point (t_0, x_0) in $]0,T[\times\mathbb{R}^2$ that is a local maximum of $(u-\phi)$,

$$\frac{\partial \phi}{\partial t}(t_0,x_0) - g(x_0) \sum_{i,j=1}^{2} a_{i,j}(\nabla\phi(t_0,x_0))\phi_{x_i x_j}(t_0,x_0) - H(x_0, \nabla\phi(t_0,x_0)) \leq 0 \text{ if } |\nabla\phi(t_0,x_0)| \neq 0,$$

$$\frac{\partial \phi}{\partial t}(t_0,x_0) - g(x_0) \overline{\lim_{p\to 0}} \sum_{i,j=1}^{2} a_{i,j}(p)\phi_{x_i x_j}(t_0,x_0) \leq 0 \quad \text{if } |\nabla\phi(t_0,x_0)| = 0.$$

Similarly, we define the notion of a viscosity supersolution by changing local maximum to local minimum, ≤ 0 to ≥ 0, and $\overline{\lim}$ to $\underline{\lim}$. A viscosity solution is a continuous function that is both a sub- and a supersolution.

If V is a Banach space, we recall that $L^\infty((0,T);V)$ is the space defined by

$$L^\infty((0,T);V) = \left\{ f : (0,T) \to V \text{ such that } |f|_{L^\infty((0,T);V)} = \inf\{c; |f|_V \leq c, \text{ a.e. } t\} < \infty \right\}.$$

We may now state the main result.

Theorem 2.3.1. *Let us assume that $g \geq 0$, with g and $\sqrt{g}$ Lipschitz continuous.*

(i) Let $u_0(x)$ be the initial condition, Lipschitz continuous. Then (2.21) has a unique viscosity solution in $C([0,\infty[\times\mathbb{R}^2) \cap L^\infty((0,T);W^{1,\infty}(\mathbb{R}^2))$ for any $T < \infty$. Moreover,

$$\inf_{\mathbb{R}^2} u_0(x) \leq u(t,x) \leq \sup_{\mathbb{R}^2} u_0(x).$$

(ii) Let v be a viscosity solution of (2.21) with u_0 replaced by v_0. Then for all T in $[0,+\infty[$ we have,

$$\sup_{0\leq t\leq T} |u(t,\cdot) - v(t,\cdot)|_{L^\infty(\mathbb{R}^2)} \leq |u_0 - v_0|_{L^\infty(\mathbb{R}^2)}. \tag{2.24}$$

Proof The proof follows [3]. It is rather technical and long, and we divide it into three steps.

Step 1: Stability and uniqueness

We begin with the stability estimate (2.24), from which we will deduce the uniqueness of a solution. Let u and v be two (viscosity) solutions associated respectively with u_0 and v_0. We are interested in the maximum of $|u(t,x)-v(t,x)|$. Otherwise, we need a trick, the duplication of variables. Let us define

$$l(t,x,y) = u(t,x) - v(t,y) - \frac{1}{4\varepsilon}|x-y|^4 - \lambda t, \quad t \in [0,T],\ x,y \in \mathbb{R}^2, \tag{2.25}$$

where $\varepsilon, \lambda \in]0,+\infty[$ will be determined later. Now we are interested in the maximum of l. Let (t_0,x_0,y_0) be a maximum point of l on $[0,T]\times\mathbb{R}^2\times\mathbb{R}^2$ (ε fixed).

We claim that $t_0 = 0$. Otherwise, the maximum would be attained at some point (t_0,x_0,y_0) with $t_0 > 0$. In that case thanks to the Crandall-Ishii lemma, we can find for any $\mu > 0$ two real numbers a, b and two symmetric (2×2) matrices X and Y such that

$$a - b = \lambda, \quad \begin{pmatrix} X & 0 \\ 0 & -Y \end{pmatrix} \leq \begin{pmatrix} B+\mu B^2 & -B-\mu B^2 \\ -B-\mu B^2 & B+\mu B^2 \end{pmatrix} \tag{2.26}$$

with

$$B_{i,j} = \varepsilon^{-1}|x_0-y_0|^2\delta_{i,j} + 2\varepsilon^{-1}(x_0-y_0)_i(x_0-y_0)_j.$$

Moreover, if $x_0 \neq y_0$, one has

$$a - g(x_0)a_{i,j}(\varepsilon^{-1}|x_0-y_0|^2(x_0-y_0))X_{i,j} - H(x_0,\varepsilon^{-1}|x_0-y_0|^2(x_0-y_0)) \leq 0, \tag{2.27}$$

$$b - g(y_0)a_{i,j}(\varepsilon^{-1}|x_0-y_0|^2(x_0-y_0))Y_{i,j} - H(y_0,\varepsilon^{-1}|x_0-y_0|^2(x_0-y_0)) \geq 0. \tag{2.28}$$

In fact, if $x_0 = y_0$, the two last inequalities have to be interpreted in terms of suitable limits. In that case $B = 0$, $X \leq 0$, $Y \geq 0$ and (2.27), (2.28) can be rewritten as

$$a - g(x_0)\lim_{p\to 0} a_{i,j}(p)X_{i,j} \leq 0, \quad b - g(x_0)\lim_{p\to 0} a_{i,j}(p)Y_{i,j} \geq 0.$$

Hence in particular, $a \leq 0$, $b \geq 0$, which contradicts $a - b = \lambda > 0$. So we have $x_0 \neq y_0$.

Next, we choose $\mu = \varepsilon|x_0-y_0|^{-2}$ (which is now possible) and deduce from (2.26)

$$\begin{pmatrix} X & 0 \\ 0 & -Y \end{pmatrix} \leq 2\varepsilon^{-1}\begin{pmatrix} C & -C \\ -C & C \end{pmatrix}, \tag{2.29}$$

where $c_{i,j} = |x_0-y_0|^2\delta_{i,j} + 5(x_0-y_0)_i(x_0-y_0)_j$. Then we set

$$G = \begin{pmatrix} g(x_0)A & \sqrt{g(x_0)g(y_0)}A \\ \sqrt{g(x_0)g(y_0)}A & g(y_0)A \end{pmatrix},$$

where $A = a_{i,j}(\varepsilon^{-1}|x_0-y_0|^2(x_0-y_0))$. G is a nonnegative symmetric matrix, so that multiplying (2.29) on the left by G and taking the trace we get

$$g(x_0)\sum_{i,j} a_{i,j}X_{i,j} - g(y_0)\sum_{i,j} a_{i,j}Y_{i,j} \leq 2\varepsilon^{-1}(\sqrt{g(x_0)} - \sqrt{g(y_0)})^2\,\mathrm{trace}(AC). \tag{2.30}$$

Next, combining (2.26), (2.27), (2.28), (2.30) and carrying out some manipulations we obtain

$$\lambda \le c_1 \varepsilon |x_0 - y_0|^4, \tag{2.31}$$

where c_1 is a constant depending only on $a_{i,j}(p)$ and g. We now estimate $|x_0 - y_0|$. According to the definition of (t_0, x_0, y_0) we have

$$u(t_0, x_0) - v(t_0, y_0) - \frac{1}{4\varepsilon}|x_0 - y_0|^4 - \lambda t_0 \ge u(t_0, y_0) - v(t_0, y_0) - \lambda t_0$$

and thus

$$\frac{1}{4\varepsilon}|x_0 - y_0|^4 \le c_2 |x_0 - y_0|, \tag{2.32}$$

where c_2 is the Lipschitz constant of $u(t_0, \cdot)$ on $[0, T] \times \mathbb{R}^2$. Therefore, from (2.31)

$$\lambda \le c_3 \varepsilon^{1/3} \quad \text{with } c_3 = c_1 4^{4/3} c_2^{4/3}.$$

Now, recall that λ and ε are arbitrary. Without loss of generality we may suppose that $\sup_{[0,T]\times\mathbb{R}^2} |u - v| \ne 0$ (otherwise, we are done), and we choose

$$\varepsilon^{1/3} = \frac{\delta}{\sup_{[0,T]\times\mathbb{R}^2} |u - v|} \quad (\delta > 0), \tag{2.33}$$

$$\lambda = \frac{2\delta c_3}{\sup_{[0,T]\times\mathbb{R}^2} |u - v|}. \tag{2.34}$$

This choice contradicts (2.32), and so $t_0 = 0$.

Next let us estimate $\sup_{[0,T]\times\mathbb{R}^2} |u - v|$. We fix λ and ε as before. Since $t_0 = 0$, we have for all (t, x, y),

$$u(t, x) - v(t, y) - \frac{1}{4\varepsilon}|x - y|^4 - \lambda t \le u_0(x_0) - v_0(y_0) - \frac{1}{4\varepsilon}|x_0 - y_0|^4, \tag{2.35}$$

but observing that

$$u_0(x_0) - v_0(y_0) = u_0(y_0) - v_0(y_0) + u_0(x_0) - u_0(y_0) \le |u_0(y_0) - v_0(y_0)| + c_2 |x_0 - y_0|$$

and letting $x = y$ in (2.35), we get

$$\sup_{[0,T]\times\mathbb{R}^2} (u(t, x) - v(t, x)) - \lambda t \le \sup_{y\in\mathbb{R}^2} |u_0(y) - v_0(y)| + \sup_{r>0} \left(c_2 r - \frac{1}{4\varepsilon} r^4 \right),$$

i.e.,

$$\sup_{[0,T]\times\mathbb{R}^2} (u(t, x) - v(t, x)) - \lambda t \le \sup_{y\in\mathbb{R}^2} |u_0(y) - v_0(y)| + \frac{3}{4} c_2^{4/3} \varepsilon^{1/3}.$$

By (2.33) and (2.34) we obtain

$$\sup_{[0,T]\times\mathbb{R}^2} (u - v) \le \sup_{y} |u_0(y) - v_0(y)| + \frac{3}{4} c_2^{4/3} \delta \sup_{[0,T]\times\mathbb{R}^2} |u - v| + 2\delta c_3 \sup_{[0,T]\times\mathbb{R}^2} |u - v| T.$$

Exchanging the role of u and v and letting $\delta \to 0$, we obtain

$$\sup_{[0,T]\times\mathbb{R}^2} |u-v| \le \sup_y |u_0(y) - v_0(y)|.$$

This proves part (ii) of Theorem 2.3.1 and the uniqueness in part (i). Observe that by using the definition of viscosity solutions we may also obtain the following bound: $\inf u_0(x) \le u(t,x) \le \sup u_0(x)$ for all (t,x).

We now prove the existence part of the theorem. We begin by setting an a priori estimate on ∇u.

Step 2: Estimate of ∇u on $L^\infty(\mathbb{R}^2)$

In this step we suppose that all the coefficients of (2.21) have been smoothed as much as necessary (notation is unchanged) and that (2.21) admits a regular solution (we will return to this question in step 3). Thus let u be a regular solution of

$$\frac{\partial u}{\partial t} = g(x)\sum_{i,j} a_{i,j}(\nabla u)u_{x_i x_j} + H(x,\nabla u).$$

We are going to apply the classical Bernstein method and derive a parabolic inequality for $w = |\nabla u|^2$. To this end we differentiate (2.21) with respect to x_l:

$$\frac{\partial u_{x_l}}{\partial t} - \frac{\partial g}{\partial x_l}\sum_{i,j} a_{i,j}(\nabla u)u_{x_i x_j} - g\left(\sum_{i,j}\sum_k \frac{\partial a_{i,j}(\nabla u)}{\partial p_k} u_{x_k x_l} u_{x_i x_j} + a_{i,j}(\nabla u)u_{x_l x_i x_j}\right) - \frac{\partial H}{\partial x_l} - \sum_k \frac{\partial H}{\partial p_k} u_{x_k x_l} = 0.$$

We multiply this equation by $2u_{x_l}$ and sum over l to obtain

$$\begin{aligned} &\tfrac{\partial w}{\partial t} - g\left(\textstyle\sum_{i,j} a_{i,j}(\nabla u)w_{x_i x_j} + \sum_{i,j}\sum_k \frac{\partial a_{i,j}(\nabla u)}{\partial p_k} u_{x_i x_j} w_{x_k}\right) - \sum_k \frac{\partial H}{\partial p_k} w_{x_k} \\ &= 2\textstyle\sum_l \frac{\partial g}{\partial x_l} u_{x_l} \sum_{i,j} a_{i,j}(\nabla u)u_{x_i x_j} - 2\sum_l \frac{\partial H}{\partial x_l} u_{x_l} - 2g\sum_l\sum_{i,j} a_{i,j}(\nabla u)u_{x_l x_i} u_{x_l x_j}, \end{aligned} \tag{2.36}$$

where $w = |\nabla u|^2$. We denote by $\mathscr{L}w$ the left-hand side of (2.36). On the other hand, for the right-hand side of (2.36), since g is smooth, we have the following:

(i) $\sum_l u_{x_l}\frac{\partial H}{\partial x_l} = \sum_l u_{x_l}\left(\alpha \frac{\partial g}{\partial x_l}|\nabla u| + \sum_i \frac{\partial^2 g}{\partial x_i \partial x_l} u_{x_i}\right) \le k_1 |\nabla u|^2 = k_1 w$, where k_1 is a constant depending only on g.

(ii) Since the matrix $a_{i,j}$ is symmetric semidefinite, we can reduce it to its principal axes, and we easily obtain

$$\left(\sum_{i,j} a_{i,j}u_{x_i}u_{x_j}\right)^2 \le k_2 \sum_k\sum_{i,j} a_{i,j}u_{x_i x_k}u_{x_j x_k} \text{ for some constant } k_2.$$

Using the Cauchy-Schwarz inequality, the obvious inequality $2ab \le a^2 + b^2$, and again that $a_{i,j}$ is symmetric semidefinite, we obtain

$$2\sum_k \frac{\partial g}{\partial x_k} u_{x_k} \sum_{i,j} a_{i,j}u_{x_i x_j} - 2g\sum_k\sum_{i,j} a_{i,j}u_{x_i x_k}u_{x_j x_k} \le k_3 w.$$

Inserting these bounds in (2.36), we have just proved the existence of a constant $k_3 > 0$ such that $\mathscr{L} w \le k_3 w$. Unfortunately, since $k_3 > 0$, we cannot directly apply the maximum principle to get a result of the kind $|w(t,\cdot)|_{L^\infty(\mathbb{R}^2)} \le |w_0(\cdot)|_{L^\infty(\mathbb{R}^2)}$ a.e. However, we can still show that (see the remark at the end of this proof)

$$|w(t,\cdot)|_{L^\infty(\mathbb{R}^2)} \le (1 + cte^{ct})|w_0(\cdot)|_{L^\infty(\mathbb{R}^2)} \text{ a.e.},$$

where c is a constant depending only on k_3. For u this means

$$|\nabla u(t,\cdot)|_{L^\infty(\mathbb{R}^2)} \le k|\nabla u_0|_{L^\infty(\mathbb{R}^2)}, \tag{2.37}$$

where the constant k depends only on $|g|_{L^\infty(\mathbb{R}^2)}$, $|\nabla g|_{L^\infty(\mathbb{R}^2)}$, and T. In particular, k does not depend on the way the coefficients have been regularized. This inequality is proved in the remark following the proof. Notice that this result is interesting only because we consider t bounded.

Step 3: Approximation and existence of a viscosity solution

In order to conclude, we are going to approximate (2.21) by a similar equation for which we are able to prove the existence of a smooth solution satisfying (2.37). To this end we consider a periodic C^∞ function u_0^ε such that $u_0^\varepsilon \to u_0$ uniformly satisfying

$$|\nabla u_0^\varepsilon|_{L^\infty(\mathbb{R}^2)} \le |\nabla u_0|_{L^\infty(\mathbb{R}^2)}, \qquad |u_0^\varepsilon|_{L^\infty(\mathbb{R}^2)} \le |u_0|_{L^\infty(\mathbb{R}^2)}.$$

We also replace $a_{i,j}$, g, and H respectively by

$$a_{i,j}^\varepsilon(p) = \varepsilon\delta_{i,j} + \delta_{i,j} - \frac{p_i p_j}{|p|^2+\varepsilon},$$

$$g^\varepsilon = g + \varepsilon,$$

$$H^\varepsilon(x,p) = \alpha g^\varepsilon(x)\sqrt{|p|^2+\varepsilon} + \sum_i \frac{\partial g^\varepsilon}{\partial x_i}(x) p_i.$$

According to the general theory of quasilinear parabolic equations [10], we know there exists a smooth solution u^ε of

$$\begin{cases} \frac{\partial u}{\partial t} = g^\varepsilon(x)\sum_{i,j} a_{i,j}^\varepsilon(\nabla u) u_{x_i x_j} + H^\varepsilon(x,\nabla u), \\ u(0,x) = u_0^\varepsilon(x). \end{cases} \tag{2.38}$$

Thanks to (2.37) we have

$$|\nabla u^\varepsilon(t,\cdot)|_{L^\infty(\mathbb{R}^2)} \le k|\nabla u_0|_{L^\infty(\mathbb{R}^2)} \equiv c_T.$$

This means that

$$|u^\varepsilon(t,x) - u^\varepsilon(t,y)| \le c_T|x-y| \quad \text{for all } t \in [0,T] \text{ and } x,y \in \mathbb{R}^2. \tag{2.39}$$

We can also show from (2.38) and (2.39) that

$$|u^\varepsilon(t,x) - u^\varepsilon(s,x)| \le c_T|t-s|^{1/2} \quad \text{for all } t,s \in [0,T] \text{ and } x \in \mathbb{R}^2. \tag{2.40}$$

Inequalities (2.39) and (2.40) together with $|u|_{L^\infty((0,T)\times\mathbb{R}^2)} \leq$ cte allow us to conclude by means of the Arzelà-Ascoli theorem that there exists a subsequence of u^ε converging uniformly on $[0,T]\times\mathbb{R}^2$ to a function $u \in C[(0,T)\times\mathbb{R}^2] \cap L^\infty[(0,T); W^{1,\infty}(\mathbb{R}^2)]$ for $T < \infty$. Then by applying a stability result for viscosity solutions we conclude that u is a viscosity of (2.21). ■

Remark (About the maximum principle in the parabolic case)

Most uniqueness results for linear parabolic (or elliptic) PDEs follow from maximum or comparison principles. Roughly speaking, they state that if u is a solution of a parabolic PDE on $U_T = (0,T)\times U$, then the maximum and the minimum of u are attained on the parabolic boundary of U_T defined by $\Gamma_T = (0,T)\times\partial U \cup \{t=0\}\times U$. More precisely, let us consider the operator

$$Lu = -\sum_{i,j} a_{i,j} u_{x_i x_j} + \sum_i b_i u_{x_i}$$

with $\sum_{i,j} a_{i,j}\xi_i\xi_j \geq \theta|\xi|^2\ \forall (t,x) \in U_T$, $a_{i,j}, b_i$ continuous and U bounded. If u is a regular solution of $u_t + Lu \leq 0$, then we have [6]

$$\max_{\overline{U_T}} u = \max_{\Gamma_T} u.$$

Likewise, if $u_t + Lu \geq 0$, then we have [6]

$$\min_{\overline{U_T}} u = \min_{\Gamma_T} u.$$

So it is clear that if two solutions coincide on Γ_T, they coincide on $\overline{U_T}$.

From the above result we can deduce the following corollaries:

- Let $\tilde{u}$ be such that
$$\begin{cases} l\tilde{u}_t + L\tilde{u} = g(t) \geq 0, \\ \tilde{u}(0,x) = u_0(x). \end{cases}$$
Then $\tilde{u} = v + \int_0^t g(s)ds$, where v is the solution of
$$\begin{cases} lv_t + Lv = 0, \\ v(0,x) = u_0(x). \end{cases}$$
So we have $\min_x u_0(x) \leq v(t,x) \leq \max_x u_0(x)$.

- Let us consider
$$\begin{cases} lu_t + Lu \leq g(t) = \tilde{u}_t + L\tilde{u}, \\ \tilde{u}(0,x) = u_0(x). \end{cases}$$
This can be rewritten as
$$\begin{cases} l(u-\tilde{u})_t + L(u-\tilde{u}) \leq 0, \\ (u-\tilde{u})(0,x) = 0. \end{cases}$$
Thanks to the maximum principle, we have $\max_{\overline{U_T}}(u-\tilde{u}) = \max_{\Gamma_T}(u-\tilde{u}) = 0$. That is, $u \leq \tilde{u}$.
But
$$\tilde{u} = v + \int_0^t g(s)ds \leq |u_0|_{L^\infty(U_T)} + \int_0^t g(s)ds,$$

so we have

$$u \leq |u_0|_{L^\infty(U_T)} + \int_0^t g(s)ds.$$

- Finally, let us consider

$$\begin{cases} lw_t + Lw \leq cw & \text{with } c \geq 0, \\ w(0,x) = u_0(x). \end{cases}$$

The classical maximum principle can no longer be applied (because $c \geq 0$). However, we have $w_t + Lw \leq c \max_x w(t,x) = g(t)$, so

$$w(t,x) \leq |u_0|_{L^\infty(U)} + c\int_0^t \max_x w(x,s)ds,$$

and then

$$|w|_{L^\infty(U)}(t) \leq |u_0|_{L^\infty(U)} + c\int_0^t |w|_{L^\infty(U)}(s)ds.$$

By applying the Gronwall inequality, we obtain

$$|w|_{L^\infty(U)}(t) \leq |u_0|_{L^\infty(U)}(1 + cte^{ct}) \leq k|u_0|_{L^\infty(U)},$$

with k depending on c and T. Observe that on $\partial(0,T) \times U$ we can choose Neumann or periodic boundary conditions.■

Finally, we would like to check the correctness of the geometric model, that is, to show that the zero-level set of $u(t,x)$ asymptotically fits the desired contour $\Gamma = \{x \in [0,1]^2; g(x) = 0\}$. Let us recall a result proven in [3]. We assume that Γ is smooth and separates $[0,1]^2$ into two regions: the inside $I(\Gamma)$ and the outside $E(\Gamma)$ (i.e., Γ is a Jordan curve). We recall that $\mathscr{P}(\mathbb{R}^N)$, the set of all subsets of $\mathbb{R}^N$, can be equipped with the Hausdorff metric

$$d(A,B) = \max\left\{\sup_{x\in A} d(x,B), \sup_{x\in B} d(x,A)\right\},$$

where $d(x,A)$ denotes as usual the distance of the point x to the set A: $d(x,A) = \inf_{y\in A} d(x,y)$.

Theorem 2.3.2. *[3]*

Let $\Gamma = \{x \in [0,1]^2; g(x) = 0\}$ be a Jordan curve of class C^2 and $\nabla g(x) = 0$ on Γ. Assume that $u_0(x)$ is smooth and bounded and that the set $\{x \in \mathbb{R}^2; u_0(x) \leq 0\}$ contains Γ and its interior. Let $u(t,x)$ be the viscosity solution of (2.21) and $\Gamma(t) = \{x; u(t,x) = 0\}$. Then if α (the constant component of the velocity) is sufficiently large, $\Gamma(t) \to \Gamma$ as $t \to +\infty$ in the Hausdorff metric.

Chapter 3

Numerical Implementation and Experiments

The Geodesic Active Contour model leads to a nonlinear partial differential equation of Hamilton-Jacobi type coupled with curvature-dependent diffusion terms. Analytical solutions are generally not available, which makes numerical approximation essential.

3.1 Finite Differences Discretization

Consider a rectangular image domain Ω discretized into a uniform grid with spacing $h_x = h_y = h$. Let $u_{i,j}^n$ denote the numerical approximation of the level set function at node (i, j) and time level n.

Spatial Derivatives

First-order derivatives are approximated using finite differences. Forward and backward differences:

$$D_x^+ u_{i,j} = \frac{u_{i+1,j} - u_{i,j}}{h}, \quad D_x^- u_{i,j} = \frac{u_{i,j} - u_{i-1,j}}{h},$$
$$D_y^+ u_{i,j} = \frac{u_{i,j+1} - u_{i,j}}{h}, \quad D_y^- u_{i,j} = \frac{u_{i,j} - u_{i,j-1}}{h}.$$

In addition to first-order derivatives, second-order spatial derivatives are required for the discretization of curvature-related terms. These derivatives are approximated using central finite differences.

The second-order derivatives in the x and y directions are given by

$$D_{xx} u_{i,j} = \frac{u_{i+1,j} - 2u_{i,j} + u_{i-1,j}}{h^2}, \qquad D_{yy} u_{i,j} = \frac{u_{i,j+1} - 2u_{i,j} + u_{i,j-1}}{h^2}.$$

The mixed derivative is approximated as

$$D_{xy} u_{i,j} = \frac{u_{i+1,j+1} - u_{i+1,j-1} - u_{i-1,j+1} + u_{i-1,j-1}}{4h^2}.$$

These approximations are used in the computation of curvature terms appearing in geometric flows such as the mean curvature motion and the geodesic active contour model.

Time Discretization

A forward Euler scheme is used for temporal evolution:

$$u^{n+1} = u^n + \Delta t \mathscr{F}(u^n),$$

where $\mathscr{F}$ denotes the spatial operator associated with the underlying evolution equation (e.g., GAC model).

The time step Δt must satisfy stability restrictions of CFL type, depending on the nature of the considered flow.

3.2 Numerical Scheme for the Geodesic Active Contour

In this section we discuss the discretization of the PDEs governing curve evolution. We examine only the case where these curves are identified as level sets of the same function $u(t,x)$ (Eulerian formulation). Of course, we have in mind the geodesic active contours model given by (2.20)

$$\frac{\partial u}{\partial t} = g(|\nabla I|)|\nabla u| \operatorname{div}\left(\frac{\nabla u}{|\nabla u|}\right) + \alpha g(|\nabla I|)|\nabla u| + \nabla g.\nabla u, \tag{3.1}$$

As mentioned before, (3.1) involves two kinds of terms: a parabolic term (the first one) and hyperbolic terms (the last two). One can easily imagine that the discretization of each term needs an appropriate treatment, according to its nature (parabolic or hyperbolic). The main idea is that parabolic terms can be discretized by central finite differences, while hyperbolic terms need to be approximated by nonoscillatory upwind schemes.

For the sake of clarity we start by examining the evolution driven by each of these terms. The decomposition of the GAC equation into simpler model equations is not only useful from a numerical perspective, but also provides insight into the specific role played by each component of the contour evolution. We therefore examine separately the curvature motion, the constant normal propagation term, and the advection term before combining them into a complete numerical scheme.

Mean Curvature Motion

Consider the mean curvature motion equation

$$\begin{cases} \dfrac{\partial u}{\partial t} = |\nabla u| \operatorname{div}\left(\dfrac{\nabla u}{|\nabla u|}\right), \\ u(0,x,y) = u_0(x,y). \end{cases} \tag{3.2}$$

This equation describes the evolution of the level sets of u under their mean curvature. Since it is a nonlinear parabolic equation, its behavior is essentially diffusive, similarly to the heat equation. Consequently, standard central finite-difference approximations are generally employed for

the spatial derivatives rather than upwind schemes, which are primarily designed for hyperbolic transport equations.

Using an explicit Euler discretization in time, the numerical scheme reads

$$u_{i,j}^{n+1} = u_{i,j}^{n} + \Delta t \, |\nabla_h u_{i,j}^{n}| \, K_{i,j}^{n},$$

where

$$|\nabla_h u_{i,j}^{n}| = \sqrt{(D_x u_{i,j}^{n})^2 + (D_y u_{i,j}^{n})^2},$$

and $K_{i,j}^{n}$ denotes a finite-difference approximation of the curvature

$$K = \operatorname{div}\left(\frac{\nabla u}{|\nabla u|}\right).$$

Expanding the divergence operator yields

$$K = \frac{u_{xx}u_y^2 + u_{yy}u_x^2 - 2u_x u_y u_{xy}}{(u_x^2 + u_y^2)^{3/2}}.$$

The second-order derivatives u_{xx}, u_{yy} and u_{xy} are approximated by central differences. This curvature term acts as a geometric diffusion operator: regions with high curvature evolve faster than flatter regions, leading to the progressive smoothing of the level-set contours while preserving their geometric structure.

Constant Speed Evolution

Another fundamental example of front propagation is the constant-speed evolution equation

$$\begin{cases} \dfrac{\partial u}{\partial t} = c\,|\nabla u|, \\ u(0,x,y) = u_0(x,y), \end{cases} \tag{3.3}$$

where c is a constant velocity. This equation describes the motion of the level sets of u in the normal direction with uniform speed c. In the corresponding Lagrangian formulation, the evolving front $\Gamma(t)$ satisfies

$$\frac{\partial \Gamma}{\partial t}(t,p) = c\,N(t,p),$$

where $N(t,p)$ denotes the unit normal vector to the front.

If $c > 0$, the front propagates outward, whereas for $c < 0$ it propagates inward. The magnitude $|c|$ determines the propagation speed, which is independent of the local geometry of the front.

This equation is a first-order Hamilton–Jacobi equation and represents one of the simplest models of interface evolution. In contrast to mean curvature motion, no smoothing mechanism is present; therefore, the shape of the evolving front is transported solely by the normal propagation velocity. The particular case $c = 1$ is often referred to as the *grass-fire model*, since it mimics the propagation of a fire front through a homogeneous medium. In this interpretation, the evolving interface

represents the boundary between the burned and unburned regions, advancing everywhere with the same speed.

From a numerical viewpoint, equation (3.3) requires a monotone upwind discretization in order to select the correct viscosity solution and avoid spurious oscillations. A commonly used choice is the Godunov scheme.

For $c > 0$, an explicit discretization reads

$$u_{i,j}^{n+1} = u_{i,j}^{n} + \Delta t\, c\, \nabla^{+} u_{i,j}^{n},$$

where

$$\nabla^{+} u_{i,j}^{n} = \Big[\max(D_x^{-} u_{i,j}^{n}, 0)^2 + \min(D_x^{+} u_{i,j}^{n}, 0)^2 + \max(D_y^{-} u_{i,j}^{n}, 0)^2 + \min(D_y^{+} u_{i,j}^{n}, 0)^2 \Big]^{1/2}.$$

Here, $D_x^{\pm}$ and $D_y^{\pm}$ denote the forward and backward finite-difference operators. This discretization is consistent with the viscosity-solution framework and provides a stable approximation of the outward normal propagation.

For $c < 0$, the upwind directions are reversed, leading to

$$\nabla^{-} u_{i,j}^{n} = \Big[\min(D_x^{-} u_{i,j}^{n}, 0)^2 + \max(D_x^{+} u_{i,j}^{n}, 0)^2 + \min(D_y^{-} u_{i,j}^{n}, 0)^2 + \max(D_y^{+} u_{i,j}^{n}, 0)^2 \Big]^{1/2}.$$

Pure Advection Equation

We now consider the linear transport equation

$$\begin{cases} \dfrac{\partial u}{\partial t} = A(x,y) \cdot \nabla u, \\ u(0,x,y) = u_0(x,y), \end{cases} \tag{3.4}$$

where $A(x,y) = \big(A_1(x,y), A_2(x,y)\big)$ is a prescribed velocity field.

Equation (3.4) is a first-order hyperbolic equation describing the transport of information along the vector field A. To obtain a stable approximation consistent with the direction of propagation, an upwind finite-difference scheme is employed. Depending on the sign of each component of the velocity field, forward or backward differences are selected, yielding

$$\begin{aligned} u_{i,j}^{n+1} = u_{i,j}^{n} + \Delta t \Big[& \max((A_1)_{i,j}^{n}, 0)\, D_x^{-} u_{i,j}^{n} + \min((A_1)_{i,j}^{n}, 0)\, D_x^{+} u_{i,j}^{n} \\ & + \max((A_2)_{i,j}^{n}, 0)\, D_y^{-} u_{i,j}^{n} + \min((A_2)_{i,j}^{n}, 0)\, D_y^{+} u_{i,j}^{n} \Big]. \end{aligned}$$

where $D_x^{\pm}$ and $D_y^{\pm}$ denote the forward and backward finite-difference operators in the x- and y-directions, respectively.

Geodesic Active Contour Model

We now consider the level-set formulation of the Geodesic Active Contour (GAC) model introduced in (3.1):

$$\frac{\partial u}{\partial t} = g\,|\nabla u|\,\kappa + \alpha g\,|\nabla u| + \nabla g \cdot \nabla u,$$

where

$$\kappa = \operatorname{div}\left(\frac{\nabla u}{|\nabla u|}\right).$$

This evolution equation naturally combines three distinct mechanisms:

- a curvature-dependent diffusion term $g\,|\nabla u|\,\kappa$, which regularizes the contour and promotes smooth boundaries;
- a constant normal propagation term $\alpha g\,|\nabla u|$, which drives the contour inward or outward;
- an advection term $\nabla g \cdot \nabla u$, which attracts the evolving contour toward image edges.

Consequently, the numerical approximation is obtained by combining the finite-difference discretizations previously derived for mean-curvature motion, constant-speed propagation, and pure advection. The resulting explicit scheme is

$$\begin{aligned} u_{i,j}^{n+1} = u_{i,j}^{n} + \Delta t \Big[& g_{i,j}\, K_{i,j}^{n} \sqrt{(D_x u_{i,j}^{n})^2 + (D_y u_{i,j}^{n})^2} \\ & + \alpha \Big(\max(g_{i,j},0)\, \nabla^{+} u_{i,j}^{n} + \min(g_{i,j},0)\, \nabla^{-} u_{i,j}^{n} \Big) \\ & + \max(g_{x,i,j},0)\, D_x^{-} u_{i,j}^{n} + \min(g_{x,i,j},0)\, D_x^{+} u_{i,j}^{n} \\ & + \max(g_{y,i,j},0)\, D_y^{-} u_{i,j}^{n} + \min(g_{y,i,j},0)\, D_y^{+} u_{i,j}^{n} \Big]. \end{aligned} \tag{3.5}$$

Here, $K_{i,j}^{n}$ denotes the finite-difference approximation of the curvature, while ∇^{+} and ∇^{-} are the Godunov upwind operators associated with outward and inward propagations, respectively. The operator ∇^{-} is obtained from ∇^{+} by interchanging the forward and backward differences.
The first term provides curvature regularization, the second term controls the normal expansion or contraction of the contour, and the last two terms constitute the edge-attraction mechanism responsible for locking the evolving interface onto object boundaries.

3.3 Experimental Results

In this section, we present numerical experiments to illustrate the behavior of the proposed implementation of the Geodesic Active Contour (GAC) model for image segmentation. The experiments are designed to examine the evolution of the level-set contour, its ability to approach object boundaries, and its behavior for images with different geometric and intensity characteristics.

The experimental study is organized into three categories. First, synthetic images are considered to illustrate the evolution of the contour in controlled settings, where the target structures have well-defined boundaries. Second, experiments on real images are presented to assess the behavior of the method on more complex image structures. Finally, challenging cases are considered to illustrate situations in which the GAC model does not accurately recover the desired boundary.
For each experiment, the initial image is displayed together with the initial contour, followed by intermediate stages of the contour evolution and the final segmentation result. The number of iterations is adapted to the evolution of the contour for each image in order to provide a clear visualization of the segmentation process. Therefore, the iteration numbers are not necessarily identical for all test images.

Experiments on Synthetic Images

Figure 3.1 presents the evolution of the GAC contour for several synthetic images. The synthetic examples provide controlled configurations for examining the ability of the level-set formulation to capture different object geometries.
For each example, the initial contour is progressively deformed under the GAC evolution and approaches the image boundaries. The intermediate results illustrate the motion of the contour, while the final result provides the corresponding binary segmentation. These experiments demonstrate the ability of the implemented scheme to handle objects with different geometrical configurations.

Experiments on Real Images

Figure 3.2 presents the segmentation results obtained on real images. Compared with the synthetic examples, these images contain more complex intensity distributions and object boundaries.
The contour evolution illustrates the ability of the GAC model to deform from the prescribed initial configuration toward image boundaries. For the tested examples, the contour reaches a stable configuration that provides a meaningful binary segmentation of the target structures.

Challenging Cases

Although the GAC model provides satisfactory results for several test images, its performance depends on the image structure and on the relationship between the initial contour and the target boundaries. Figure 3.3 presents several challenging examples for which the contour does not accurately recover the desired segmentation.

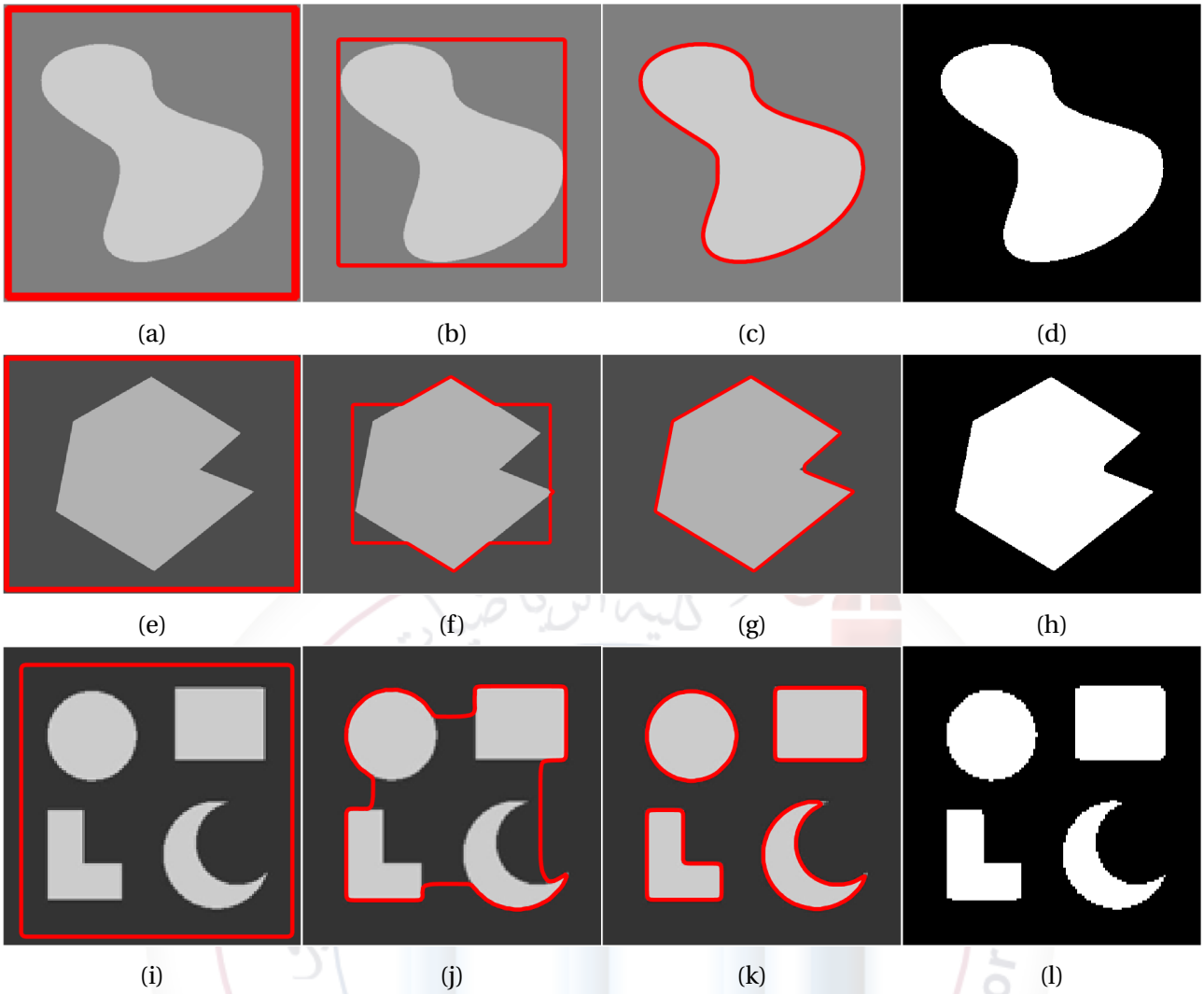


Figure 3.1: Evolution of the GAC contour on synthetic images. Left: initial image with the initial contour; middle-left and middle-right: intermediate stages of contour evolution; right: final binary segmentation result.

These examples illustrate an important limitation of edge-based active contours. When image gradients are weak, object boundaries are poorly defined, or competing edges are present, the evolving contour may stop at an undesired boundary or fail to reach the target object. The results therefore emphasize the dependence of the GAC model on the image edge indicator and on the initialization of the level-set function.

Overall, the experiments illustrate both the capabilities and the limitations of the implemented GAC model. The method can successfully capture well-defined object boundaries in several synthetic and real images, while its performance may deteriorate in the presence of weak, ambiguous, or competing edges. These observations are consistent with the edge-based nature of the GAC formulation and motivate the consideration of more robust region-based or hybrid segmentation models for challenging images.

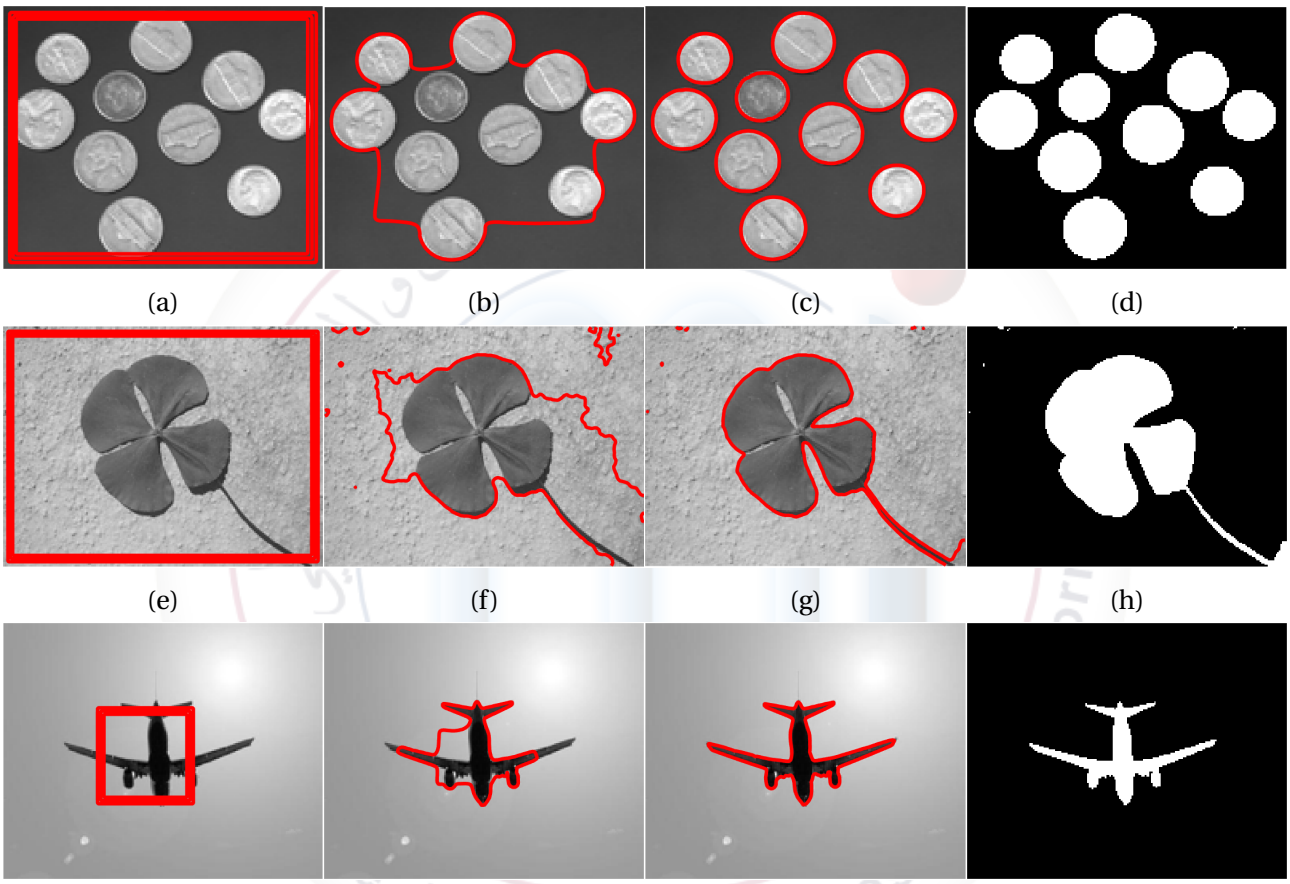


Figure 3.2: Evolution of the GAC contour on real images. Left: initial image with the initial contour; middle-left and middle-right: intermediate stages of contour evolution; right: final binary segmentation result.

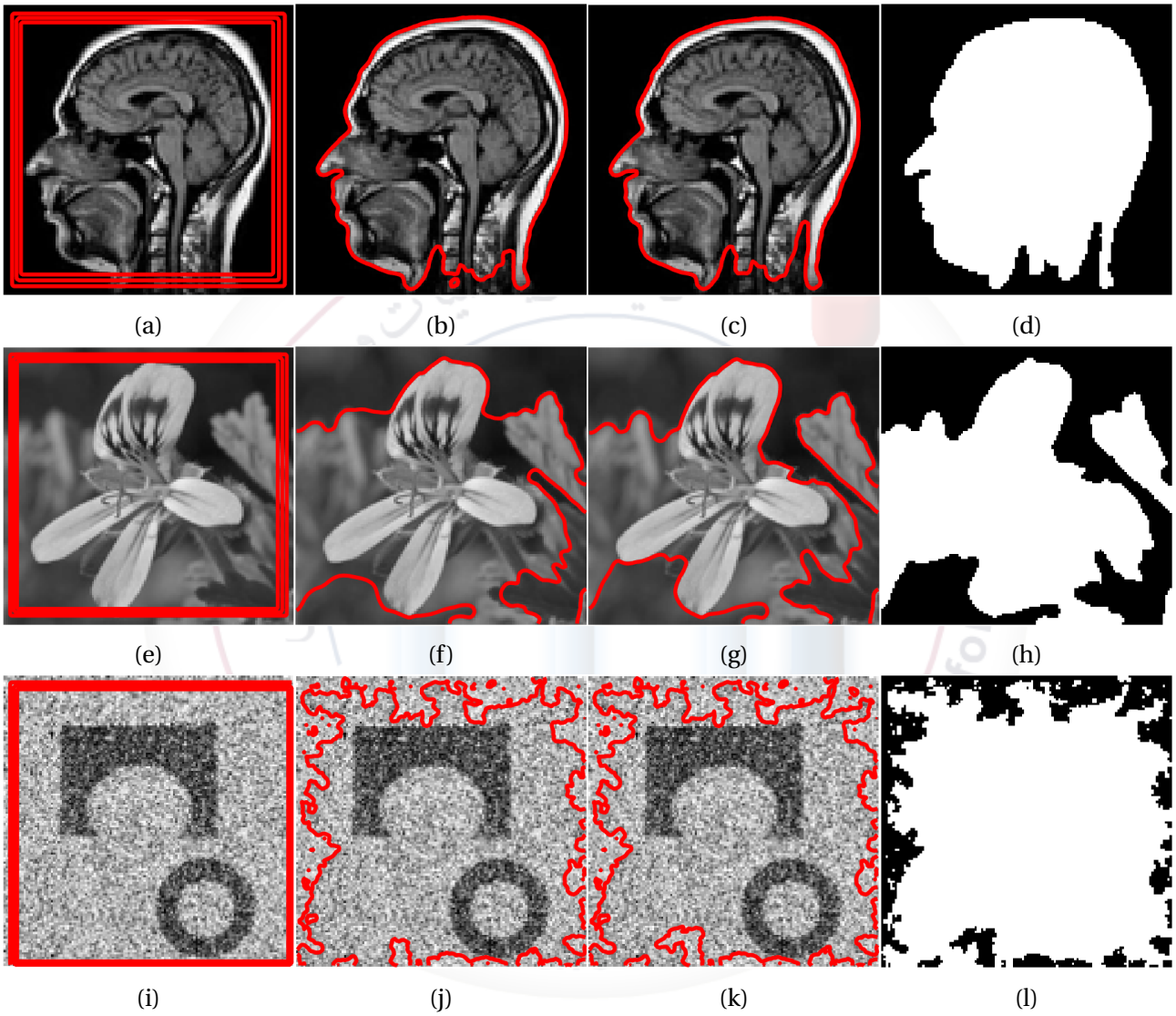


Figure 3.3: Examples of challenging cases for the GAC model. Left: initial image with the initial contour; middle-left and middle-right: intermediate stages of contour evolution; right: final binary segmentation result.

Conclusion

In this memory, we have studied the Geodesic Active Contour model for image segmentation, from its theoretical foundations to its numerical implementation, through the unifying perspective of partial differential equations.

We began, in Chapter 1, by establishing the mathematical background necessary for the rest of the work, covering the basic notions of image processing and edge detection, the elements of differential geometry related to curvature, and the essential theory of partial differential equations, including the level set method. This preliminary material provided the tools required to formulate active contour models in a rigorous mathematical setting.

In Chapter 2, we examined in detail the transition from the classical Kass–Witkin–Terzopoulos snake model to the Geodesic Active Contour model of Caselles, Kimmel, and Sapiro. We showed how the non-intrinsic, parametrization-dependent energy of the snake model can be reformulated as an intrinsic weighted length functional, and we discussed, following Aubert and Blanc-Féraud, a precise notion of equivalence between the two associated minimization problems. The resulting evolution equation was interpreted geometrically as the balance between a curvature-driven regularizing force and an edge-driven attraction force, further enhanced by a balloon term that facilitates the detection of non-convex objects. Reformulating this evolution within the level set framework led to a Hamilton–Jacobi-type parabolic equation, for which we established, in the sense of viscosity solutions, the existence, uniqueness, and stability of the solution, as well as a convergence result guaranteeing that the zero level set asymptotically approaches the true object boundary.

In Chapter 3, we translated this theoretical model into a working numerical scheme. By decomposing the governing equation into a curvature (parabolic) term, a constant propagation term, and an advection term, we were able to discretize each component according to its own mathematical nature: central finite differences for the diffusive part, and monotone upwind schemes of Godunov type for the hyperbolic parts, thereby ensuring numerical stability and consistency with the viscosity solution framework. The experiments carried out on synthetic images, real images, and challenging cases confirmed that the implemented scheme is able to accurately segment objects with well-defined boundaries, while also revealing the intrinsic limitations of purely edge-based models when confronted with weak, ambiguous, or competing gradients.

Taken together, the results obtained throughout this memory confirm that the Geodesic Active Contour model offers an elegant and mathematically well-founded framework for image segmentation, combining ideas from the calculus of variations, differential geometry, and the theory of partial differential equations. At the same time, our experimental study highlights that the performance of the model remains strongly dependent on the quality of the edge indicator function and on the initialization of the contour, which constitutes an inherent limitation of edge-based approaches.

Bibliography

[1] G. Aubert and P. Kornprobst. Mathematical Problems in Image Processing: Partial Differential Equations and the Calculus of Variations. Springer, 2006.

[2] G. Aubert and L. Blanc-Féraud. Some remarks on the equivalence between 2D and 3D classical snakes and geodesic active contours. International Journal of Computer Vision, 34(1):19-28, 1999.

[3] V. Caselles, F. Catte, T. Coll, and F. Dibos. A geometric model for active contours. Numerische Mathematik, 66:1-31, 1993.

[4] V. Caselles, R. Kimmel, and G. Sapiro. Geodesic active contours. The International Journal of Computer Vision, 22(1):61-79, 1997.

[5] A. Dervieux and F. Thomasset. A finite element method for the simulation of Rayleigh-Taylor instability. Lecture Notes in Mathematics, 771:145-159, 1979.

[6] L.C. Evans. Partial Differential Equations, volume 19 of Graduate Studies in Mathematics. Proceedings of the American Mathematical Society, 1998.

[7] M. Kass, A. Witkin, and D. Terzopoulos. Snakes: Active contour models. In First International Conference on Computer Vision, pages 259-268, London, June 1987.

[8] S. Kichenassamy, A. Kumar, P. Olver, A. Tannenbaum, and A. Yezzi. Gradient flows and geometric active contour models. In Proceedings of the 5th International Conference on Computer Vision, pages 810-815, Boston, MA, June 1995. IEEE Computer Society Press.

[9] S. Kichenassamy, A. Kumar, P. Olver, A. Tannenbaum, and A. Yezzi. Conformal curvature flows: from phase transitions to active vision. Archive for Rational Mechanics and Analysis, 134:275-301, 1996.

[10] O.A. Ladyzhenskaya, V.A. Solonnikov, and N.N. Uralćeva. Linear and Quasilinear Equations of Parabolic Type. Proceedings of the American Mathematical Society, Providence, RI, 1968.

[11] R. Malladi, J.A. Sethian, and B.C. Vemuri. Shape modeling with front propagation: A level set approach. IEEE Transactions on Pattern Analysis and Machine Intelligence, 17(2):158-175, February 1995.

[12] S. Osher and J.A. Sethian. Fronts propagating with curvature-dependent speed: Algorithms based on Hamilton-Jacobi formulations. Journal of Computational Physics, 79(1):12-49, 1988.

[13] G. Sapiro. Geometric Partial Differential Equations and Image Analysis. Cambridge University Press, 2001.

[14] J.A. Sethian. Level Set Methods and Fast Marching Methods: Evolving Interfaces in Computational Geometry, Fluid Mechanics, Computer Vision, and Materials Sciences. Cambridge Monograph on Applied and Computational Mathematics. Cambridge University Press, 1999.

Faculté des Mathématiques et de l'Informatique